

INFORMATION TO USERS

This was produced from a copy of a document sent to us for microfilming. While the most advanced technological means to photograph and reproduce this document have been used, the quality is heavily dependent upon the quality of the material submitted.

The following explanation of techniques is provided to help you understand markings or notations which may appear on this reproduction.

1. The sign or "target" for pages apparently lacking from the document photographed is "Missing Page(s)". If it was possible to obtain the missing page(s) or section, they are spliced into the film along with adjacent pages. This may have necessitated cutting through an image and duplicating adjacent pages to assure you of complete continuity.
2. When an image on the film is obliterated with a round black mark it is an indication that the film inspector noticed either blurred copy because of movement during exposure, or duplicate copy. Unless we meant to delete copyrighted materials that should not have been filmed, you will find a good image of the page in the adjacent frame.
3. When a map, drawing or chart, etc., is part of the material being photographed the photographer has followed a definite method in "sectioning" the material. It is customary to begin filming at the upper left hand corner of a large sheet and to continue from left to right in equal sections with small overlaps. If necessary, sectioning is continued again—beginning below the first row and continuing on until complete.
4. For any illustrations that cannot be reproduced satisfactorily by xerography, photographic prints can be purchased at additional cost and tipped into your xerographic copy. Requests can be made to our Dissertations Customer Services Department.
5. Some pages in any document may have indistinct print. In all cases we have filmed the best available copy.

**University
Microfilms
International**

300 N. ZEEB ROAD, ANN ARBOR, MI 48106
18 BEDFORD ROW, LONDON WC1R 4EJ, ENGLAND

8006402

JONES, DOUGLAS WAYNE

CALCULATED AND OBSERVED LINE STRENGTH RATIOS IN CESIUM II

The University of Arizona

PH.D.

1979

**University
Microfilms
International**

300 N. Zeeb Road, Ann Arbor, MI 48106

18 Bedford Row, London WC1R 4EJ, England

CALCULATED AND OBSERVED
LINE STRENGTH RATIOS IN CS II

by

Douglas Wayne Jones

A Dissertation Submitted to the Faculty of the
DEPARTMENT OF PHYSICS
In Partial Fulfillment of the Requirements
For the Degree of
DOCTOR OF PHILOSOPHY
In the Graduate College
THE UNIVERSITY OF ARIZONA

1 9 7 9

THE UNIVERSITY OF ARIZONA
GRADUATE COLLEGE

I hereby recommend that this dissertation prepared under my direction
by Douglas Wayne Jones

entitled Calculated and Observed Line Strength Ratios in Cs II

be accepted as fulfilling the dissertation requirement for the Degree
of Doctor of Philosophy.

Al Dmille
Dissertation Director

Sept 4, 1979
Date

As members of the Final Examination Committee, we certify that we have
read this dissertation and agree that it may be presented for final
defense.

Rob Stark

Sept 7, 1979
Date

M. Sargent III

Sept. 4, 1979
Date

Frederic A Hoyt

Sept. 4, 1979
Date

M. D. Scadron

Sept 4, 1979
Date

Date

Final approval and acceptance of this dissertation is contingent on the
candidate's adequate performance and defense thereof at the final oral
examination.

STATEMENT BY AUTHOR

This dissertation has been submitted in partial fulfillment of requirements for an advanced degree at The University of Arizona and is deposited in the University Library to be made available to borrowers under rules of the Library.

Brief quotations from this dissertation are allowable without special permission, provided that accurate acknowledgment of source is made. Requests for permission for extended quotation from or reproduction of this manuscript in whole or in part may be granted by the head of the major department or the Dean of the Graduate College when in his judgment the proposed use of the material is in the interests of scholarship. In all other instances, however, permission must be obtained from the author.

SIGNED: _____

Douglas Jones

ACKNOWLEDGMENTS

I am deeply grateful to the following friends for their valuable assistance:

John McCullen, scholar and advisor extraordinaire,

Dave Anderson, George Dezenberg and Art Smith, tireless co-workers who cared,

Kathy Huppe, my loving and understanding wife,

Maryellen Peck, a dear and empathetic friend,

Mary Anne Meyer, for carefully typing this text and making many helpful suggestions and corrections and

John Howe, for skillfully drafting the illustrations herein.

TABLE OF CONTENTS

	Page
LIST OF TABLES	v
LIST OF ILLUSTRATIONS	vi
ABSTRACT	vii
1. INTRODUCTION	1
2. CALCULATION OF LINE STRENGTHS	3
Estimation of Radial Integrals	7
3. MEASUREMENT OF LINE STRENGTH RATIOS	14
The Cs II Lamp	19
Pulsed Gas Valve and Plasma Gun	22
Cs Vapor Source	27
Spectrographic and Photometric Techniques	31
4. RESULTS AND CONCLUSIONS	36
Calculated Cs II Line Strengths	36
Comparison of Observed and Calculated Ratios	47
Conclusions	52
APPENDIX A: NEW ENERGY LEVELS AND CLASSIFICATIONS IN CS II .	57
APPENDIX B: GENERAL SOLUTIONS OF THE RADIAL WAVE EQUATION . .	61
REFERENCES	67

LIST OF TABLES

Table	Page
I. Cs II Line Strengths: $5d, 6s \frac{1}{2} [K]_J - 6p \frac{1}{2} [K']_{J_1}$	39
II. Cs II Line Strengths: $5d, 6s \frac{1}{2} [K]_J - 6p 1 \frac{1}{2} [K']_{J_1}$	40
III. Cs II Line Strengths: $5d, 6s 1 \frac{1}{2} [K]_J - 6p \frac{1}{2} [K']_{J_1}$	41
IV. Cs II Line Strengths: $5d, 6s 1 \frac{1}{2} [K]_J - 6p 1 \frac{1}{2} [K']_{J_1}$	42
V. Cs II Line Strengths: $6p \frac{1}{2} [K]_J - 6d, 7s \frac{1}{2} [K']_{J_1}$	43
VI. Cs II Line Strengths: $6p \frac{1}{2} [K]_J - 6d, 7s 1 \frac{1}{2} [K']_{J_1}$	44
VII. Cs II Line Strengths: $6p 1 \frac{1}{2} [K]_J - 6d, 7s \frac{1}{2} [K']_{J_1}$	45
VIII. Cs II Line Strengths: $6p 1 \frac{1}{2} [K]_J - 6d, 7s 1 \frac{1}{2} [K']_{J_1}$	46
IX. Comparison of Observed and Calculated Line Strength Ratios in Cs II	49
X. New Energy Levels in Cs II	59
XI. New Classifications in Cs II	60

LIST OF ILLUSTRATIONS

Figure	Page
1. Schematic Diagram of Apparatus	15
2. Diagram of Pulsed Gas Valve and Plasma Gun	23
3. Diagram of Cs Vapor Source	28
4. Plot of Film Characteristics	34

ABSTRACT

Calculated and observed line strength ratios for selected electric dipole allowed transitions in the spectrum of Cs II are presented in this dissertation. The calculated values are obtained by employing a novel theoretical approach called the effective Coulomb potential (ECP) approximation. This new approximation is contrasted with the standard Coulomb approximation. The ECP results, which are consistent in relative phase with standard self-consistent field calculations, are used in the multiconfiguration approximation to the energy levels of Cs II. Absolute line strengths as given by the ECP approximation are tabulated for all the transitions 5d-6p, 6s-6p, 6p-6d and 6p-7s in Cs II.

For selected strong lines in the spectrum of Cs II, line strength ratios were measured. The ECP predictions are found to agree favorably with the experimentally measured ratios. The measured values were obtained by standard spectrographic and photometric techniques from a Cs II lamp of novel design. This lamp operates in an electrodeless, beam clashing mode in which a hot, free plasma pulse collides with a very dense, cool vapor of neutral atomic Cs.

Evidence for the identification of five new energy levels and for the classification of 19 previously unclassified lines in Cs II is presented in an appendix. A second appendix considers the general solutions of the radial wave equation in some detail.

CHAPTER 1

INTRODUCTION

This dissertation presents a comparison of calculated and observed line strength ratios for electric dipole allowed transitions in the spectrum of Cs II. The theoretical techniques employed in approximating the line strengths represent a novel approach which appears to be applicable in the multiconfigurational approximation. Chapter 2 presents the development of these techniques and compares this new approximation called the effective Coulomb potential (ECP) approximation to the commonly employed Coulomb approximation (Bates and Damgaard 1949).

The experimental methods used in measuring the line strength ratios are described in Chapter 3. The spectral intensity data were obtained by standard spectrographic and photometric techniques. The Cs II lamp used throughout this research, however, is a novel light source operating in an electrodeless, beam clashing mode. The bulk of Chapter 3 is devoted to describing this original device.

In Chapter 4, the results of this research are presented. The experimental line strength ratios are compared to the predicted values given by the ECP approximation. The absolute line strengths for all the electric dipole transitions 5d-6p, 6s-6p, 6p-6d and 6p-7s have been calculated in the ECP approximation and are tabulated in Chapter 4. Also a comparison of predicted line strengths with values derived from the intensity estimates of published line lists is put forth. In each

case of comparison mentioned above, the corresponding results in the classic Coulomb approximation are considered. It is shown that the ECP approximation gives generally better results than the Coulomb approximation though neither approximation works exceptionally well in describing Cs II.

This dissertation concludes with two appendices. Appendix A presents evidence for the identification of five new levels in Cs II and for the classification of 19 previously unclassified transitions. In Appendix B, the general solutions to the radial wave equation are considered with special emphasis on the ECP form of the equation.

CHAPTER 2

CALCULATION OF LINE STRENGTHS

The absolute line strength for an electric dipole transition by a single optical electron from the state $|E_i, J_i M_i\rangle$ to the state $|E_f, J_f M_f\rangle$ is defined as (Condon and Shortley 1970, p. 98)

$$S(E_f, E_i) = \sum_{M_f M_i q} |\langle E_f, J_f M_f | D_q | E_i, J_i M_i \rangle|^2, \quad (1)$$

where D_q is the q th component of the first rank tensor operator representing the electric dipole transition, E is the energy and JM are the total angular momentum quantum numbers of the respective states. The electric dipole transition operator is

$$D_q = \sum d_{qi}, \quad (2)$$

where d_{qi} is the single electron, electric dipole transition operator for the i th electron and where the summation is over all the electrons making up the states $|E, JM\rangle$. Transitions of higher electromagnetic multipolarity and transitions involving groups of equivalent electrons are not considered here. The extension of the present formalism to include these more complex transitions is straightforward though tedious (see, for example, Sobel'man 1972, pp. 313-35).

By defining the reduced matrix element (Brink and Satchler 1968, p. 57)

$$\langle E', J' || D || E, J \rangle = \sum_{M, q} (\langle J' M' | J 1 M q \rangle \langle E', J' M' | D_q | E, J M \rangle), \quad (3)$$

the line strength may be written as

$$S(E_f, E_i) = (2J_f + 1) |\langle E_f, J_f \| D \| E_i, J_i \rangle|^2. \quad (4)$$

If the states $|E, JM\rangle$ are built up from single electron states, they have the form of sums of products of single electron states. This, together with equation (2), allows the reduced matrix elements in equation (4) to be written as a series expansion over single electron reduced matrix elements of d_q . In the central field approximation to the individual configurations making up the single electron states, the line strength takes the form

$$S(E_f, E_i) = |\sum C(E_f, J_f; E_i, J_i | n_f l_f, n_i l_i) \langle n_f l_f \| d \| n_i l_i \rangle|^2, \quad (5)$$

where the sum is over initial and final configurations, $n l$, and where the coefficients C follow from the composition amplitudes of the $|E, JM\rangle$ and from the angular momentum recoupling algebra.

In order to clarify the meaning of C , consider a system which may be approximated as a single optical electron attached to an atomic or ionic core consisting of filled and partially filled shells. As mentioned above, transitions involving the filled and partially filled shells are specifically excluded from consideration. The excited states $|E, JM\rangle$ of such a system might be given in the LS basis set by a Hartree-Fock procedure, for example,

$$|E, JM\rangle = \sum (|\gamma n l; [[S_1 \frac{1}{2}] S [L_1 l] L] JM) \\ \times \langle \gamma n l; [[S_1 \frac{1}{2}] S [L_1 l] L] J | E, J \rangle), \quad (6)$$

where the summation is over all quantum numbers except JM and where S and L are, respectively, total spin and total orbital angular momentum quantum numbers with the subscript one denoting the core state. The coefficients C in equation (5) are given for this system by

$$\begin{aligned}
C(E', J'; E, J | n' \ell'; n \ell) &= [(2J' + 1)(2J + 1)(2\ell' + 1)]^{\frac{1}{2}} \\
&\times \Sigma \{ [(2L' + 1)(2L + 1)]^{\frac{1}{2}} W(J' 1 S L; J L') \\
&\times W(L' 1 L_1 \ell; L \ell') \langle E', J' | \gamma' n' \ell'; [[S_1^{\frac{1}{2}}] S [L_1 \ell'] L'] J' \rangle \\
&\times \langle \gamma n \ell; [[S_1^{\frac{1}{2}}] S [L_1 \ell] L] J | E, J \rangle \}, \quad (7)
\end{aligned}$$

where the summation extends over all the quantum numbers not appearing in the argument of C and where $W(abcd;ef)$ is the Racah coefficient (Brink and Satchler 1968, p. 43).

Since each individual configuration in equation (5) is computed in the central field approximation, the single electron states $|n\ell m\rangle$ have wavefunctions,

$$\langle r | n\ell m \rangle = i^{\ell} Y_{\ell m}(\theta, \phi) P_{n\ell}(r)/r, \quad (8)$$

where the $Y_{\ell m}(\theta, \phi)$ are spherical harmonics (Brink and Satchler 1968, p. 18) and the $P_{n\ell}(r)$ satisfy the radial wave equation (Sobel'man 1972, p. 341),

$$\frac{d^2 P_{n\ell}(r)}{dr^2} - 2[E_{n\ell} + V(r) - \frac{Z}{r} + \frac{\ell(\ell + 1)}{2r^2}] P_{n\ell}(r) = 0. \quad (9)$$

The energy parameter $E_{n\ell}$ is the (positive) center of gravity term value for the configuration $n\ell$. In equation (9) and throughout what follows, atomic units (Condon and Shortley 1970, p. 432) are utilized.

The difficulty in evaluating equation (9) arises from the appearance of the potential $V(r)$ which represents the net effect of the electrons other than the one under consideration. Since the form of $V(r)$ is not known, except asymptotically, various approximation techniques have been applied to its evaluation. These range in complexity from elaborate self-consistent field approaches, such as Hartree-Fock

calculations, to the maximal sort of simplification present in the Coulomb approximation of Bates and Damgaard (1949) and in the ECP approximation presented here.

In general, equation (5) can be considered to be a multiconfigurational expansion as in the example above. If, however, the single configuration approximation is valid, then the summation sign may be deleted since only one configuration will contribute to each $|E, JM\rangle$. Clearly, in this latter case, the relative phases of the reduced matrix elements can have no effect. The Coulomb approximation (Bates and Damgaard 1949) is readily applicable to these single configuration states and works amazingly well in most instances. For the former, multiconfigurational case, the relative phases of the reduced matrix elements may have a profound effect. The reduced matrix elements, in this case, should be consistent in relative phase with the phase conventions employed in determining the state amplitudes. In nearly all instances, these composition amplitudes are found from a Hartree-Fock procedure or some variation thereof. Throughout the present work, it is assumed that just such a procedure has been employed in obtaining amplitudes of the type shown in equation (6).

The single electron, electric dipole transition operator for spontaneous emission is (Brink and Satchler 1968, p. 90)

$$d_q = (-4\pi/3)^{\frac{1}{2}} Y_{1q}(\theta, \phi) r, \quad (10)$$

which with equation (8) yields

$$\begin{aligned} \langle n'l' || d || n\ell \rangle &= [\ell_M / (2\ell_M \pm 1)]^{\frac{1}{2}} I(n'l'; n\ell), \ell' = \ell \pm 1 \\ &= 0, \ell' \neq \ell \pm 1 \end{aligned} \quad (11)$$

where

$$I(n'\ell';n\ell) = \int_0^{\infty} dr P_{n'\ell'}(r)rP_{n\ell}(r) \quad (12)$$

defines the radial integral of r and where ℓ_M is the greater of ℓ and ℓ' . Thus, the crux of the line strength problem is the evaluation of the radial integrals, $I(n'\ell';n\ell)$. Equation (12) also makes the necessary phase relationships discussed above more apparent. Phase consistency in the reduced matrix elements may be insured provided the $P_{n\ell}(r)$ used in evaluating equation (12) have the same relative phases as the $P_{n\ell}(r)$ implicit in the Hartree-Fock formalism. It will be apparent from the equations discussed in the next section that the Coulomb approximation to $P_{n\ell}(r)$ does not have this property, whereas the ECP solutions do. Further, it should be noted that, though the $P_{n\ell}(r)$ are implicit to the Hartree-Fock formalism, they are not usually actually calculated. If the $P_{n\ell}(r)$ are calculated in this manner, then in most instances it is with greater than normal expense and the results are given only in cumbersome numerical form. A more simple and efficient means of estimating $P_{n\ell}(r)$, and thus $I(n'\ell';n\ell)$, is, therefore, desirable.

Estimation of Radial Integrals

In this section, the Coulomb approximation and the ECP approximation procedures for estimating the radial integrals $I(n'\ell';n\ell)$ are discussed and compared from a theoretical point of view. Both of these procedures begin with the assumption that the net potential in equation (9) may be approximated by a Coulombic potential,

$$V(r) = Z/r \sim - C/r. \quad (13)$$

This functional form is exact for hydrogenic systems and is expected to be the limiting form for high lying ($n \rightarrow \infty$) states in general. Substitution of equation (13) into equation (9) gives the basic equation for $P_{n\ell}(r)$ in both the Coulomb approximation and the ECP approximation,

$$\frac{d^2 P_{n\ell}(r)}{dr^2} - 2\left[E_{n\ell} - \frac{C}{r} + \frac{\ell(\ell+1)}{2r^2}\right]P_{n\ell}(r) = 0. \quad (14)$$

In formulating the Coulomb approximation, Bates and Damgaard (1949) further assume that the potential constant C will have the limiting value corresponding to the potential experienced by a free electron at infinity. That is, C is the integer charge excess on the ionic core when the optical electron is removed. This is justified by observing that the main contributions to the radial integral of r accumulate at relatively large radial distances. Unfortunately, if C and $E_{n\ell}$ are fixed independently, then equation (14) is not, in general, an eigenfunction equation and $P_{n\ell}(r)$ becomes a continuous function of the real parameter n^* :

$$n \rightarrow n^* = C(2E_{n\ell})^{-\frac{1}{2}}; \quad (15)$$

$$P_{n\ell}(r) \rightarrow P_{\ell}(r; n^*). \quad (16)$$

The $P_{\ell}(r; n^*)$ diverge as $r^{-\ell}$ at the origin and do not represent stationary states in the usual quantum mechanical sense. The appropriate solution which is regular at infinity is

$$P_{\ell}(r; n^*) = N W_{n^*, \ell + \frac{1}{2}}(2Cr/n^*), \quad (17)$$

where $W_{\mu, \nu}(z)$ is the Whittaker function discussed in Appendix B and the normalization constant N is

$$N = [n^{*2} \Gamma(n^* + \ell + 1) \Gamma(n^* - \ell) / C]^{-\frac{1}{2}}. \quad (18)$$

This normalization cannot be derived explicitly and was suggested intuitively by Hartree (1927) as analogous to the normalization when n^* is an integer.

The radial integrals $I(n'l';n\ell)$ are evaluated by Bates and Damgaard (1949) by substituting asymptotic expansions for large r of the functions $P_\ell(r;n^*)$ into equation (12) and termwise integrating. This leads to divergent terms in the resulting expansion. These terms correspond to integrals whose dominant contributions are close to the origin. Arguing that exclusion of the region near the origin should have a negligible effect on the actual radial integrals, Bates and Damgaard (1949) truncate the expansion one term prior to reaching a divergent term. This series truncation in effect avoids the region near the origin where $P_\ell(r;n^*)$ is divergent and acts in lieu of a cut-off distance. There is a certain arbitrariness in this procedure (Burgess and Seaton 1960), however. The final expression for the radial integral in the Coulomb approximation (Bates and Damgaard 1949, p. 104) requires the computation and accumulation of about $[(n^{*'} + n^*) (n^{*'} + n^* + 1)/2]$ terms.

The ECP approximation procedure, on the other hand, seeks solutions to equation (14) which represent stationary, bound states in the usual quantum mechanical sense. These solutions are bounded, square integrable eigenfunctions of equation (14) which satisfy the boundary conditions of vanishing at both the origin and infinity. Since, as shown in Appendix B, this class of solutions is found when n is an integer, n is assumed to retain its usual role as the principal quantum

number of the configuration $n\ell$. This fixes both n and $E_{n\ell}$, however, and leaves the potential constant C the only remaining free parameter in equation (14).

It seems reasonable to make C an adjustable real parameter C^* which, to lowest order, compensates for the deviation of the true potential from a Coulomb potential. This is accomplished by using the eigenvalue equation to determine C^* and by letting the eigenfunction solutions to equation (14) be continuous functions of this parameter:

$$C \rightarrow C^* = n(2E_{n\ell})^{\frac{1}{2}}; \quad (19)$$

$$P_{n\ell}(r) \rightarrow P_{n\ell}(r; C^*). \quad (20)$$

The basic ECP equations, (19) and (20), are the counterparts of equations (15) and (16) in the Coulomb approximation.

Physically, the ECP approximation adjusts the potential well in the vicinity of each configuration energy until, to lowest order, it yields a bound state with the correct quantum numbers and with the empirically determined energy. In a sense, the ECP approximation gives a crude, piecewise estimation of the true potential curve. As $n \rightarrow \infty$, the value of C^* is expected to asymptotically approach the integer value C , a point that is examined more closely at the end of this chapter. It also should be noted that the ECP approximation is, at least in principle, applicable to negative ions where the core is atomic ($C = 0$).

With the conditions expressed in equation (19) and (20), the ECP solutions follow immediately by analogy to the hydrogenic problem. The appropriate, normalized solution from Appendix B is

$$P_{n\ell}(r;C^*) = \frac{1}{n(2\ell+1)!} \left[\frac{C^*(n+\ell)!}{(n-\ell-1)!} \right]^{\frac{1}{2}} \left(\frac{2C^*r}{n} \right)^{\ell+1} \times \exp\left(-\frac{C^*r}{n}\right) {}_1F_1(-n+\ell+1; 2\ell+2; \frac{2C^*r}{n}), \quad (21)$$

where ${}_1F_1(a;b;z)$ is the confluent hypergeometric function (Landau and Lifshitz 1975, p. 119). Substitution of solutions $P_{n\ell}(r;C^*)$ and $P_{n'\ell-1}(r;C^{*'})$ into the radial integral equation (12) yields the Gordon integral $J_{2\ell+1}^{(1,2)}(n-\ell-1, n'-\ell)$ (Gordon 1929; Landau and Lifshitz 1975, p. 607) from which it follows that

$$I(n\ell; n'\ell-1) = - \frac{(-)^{n'} \beta^{\ell+1} \alpha^{n+n'}}{4(C^*C^{*'})^{\frac{1}{2}}(2\ell-1)!} \times \left[\frac{(n+\ell)! (n'+\ell-1)!}{(n-\ell-1)! (n'-\ell)!} \right]^{\frac{1}{2}} \left[(1-\gamma) {}_2F_1(-n+\ell+1, -n'+\ell; 2\ell; \beta) + 2\alpha\gamma {}_2F_1(-n+\ell, -n'+\ell; 2\ell; \beta) - 2\alpha^2(1+\gamma) {}_2F_1(-n+\ell-1, -n'+\ell; 2\ell; \beta) \right], \quad (22)$$

where ${}_2F_1(a,b;c;z)$ is the hypergeometric function (Landau and Lifshitz 1975, p. 605) and where

$$\alpha = (1-\rho)/(1+\rho), \quad (23)$$

$$\beta = -4\rho/(1-\rho)^2, \quad (24)$$

$$\gamma = n - n'/\rho, \quad (25)$$

with

$$\rho = (E_{n\ell}/E_{n'\ell-1})^{\frac{1}{2}}. \quad (26)$$

For hydrogenic systems ($C^* = C^{*'}$), the parameter γ vanishes and equation (22) reduces to the well-known Gordon formula (Condon and Shortley 1970, p. 131). An interesting feature of equation (22) is its ability to handle the case $n = n'$ in the hydrogenic limit,

$$\lim_{C^* \rightarrow C^{*1}} I(n\ell; n\ell - 1) = -\frac{3n}{2C^*} (n^2 - \ell^2)^{\frac{1}{2}}. \quad (27)$$

This result cannot be obtained from the Gordon formula because it is a consequence of the second term of the sum in equation (22).

The ECP procedure, therefore, permits the calculation of all radial integrals of r , exact and approximate, from a single unified expression, equation (22). Also, since each hypergeometric function is a terminating series, no ad hoc truncation is required. Evaluation of equation (22) necessitates the computation and accumulation of about $[3(n - \ell)]$ terms as compared to about $[\frac{1}{2}(n^{*1} + n^*)(n^{*1} + n^* + 1)]$ terms for the Coulomb approximation. Absolute line strengths, in the ECP approximation, are obtained by substituting equation (22) into equation (11), and the resulting expression into equation (5).

The connection between the asymptotic behavior of C^* and the empirically observed quantum defect (Sobel'man 1972, p. 40),

$$\delta_\ell = n - n_\ell^*, \quad (28)$$

is interesting also. Usually, δ_ℓ is found to be a small, positive number which becomes independent of n as n becomes large. By using the relationship

$$n_\ell^*/C = n/C^* = (2E_{n\ell})^{\frac{1}{2}}, \quad (29)$$

it is found that to $O(\delta_\ell/n)$

$$C^* = C(1 + \delta_\ell/n). \quad (30)$$

The quantum defect δ_ℓ , therefore, may be interpreted, in the ECP approximation, as the first order coefficient in an expansion describing the asymptotic behavior of C^* as $n \rightarrow \infty$. The ECP quantum numbers have

no "defect". Physically, effects such as penetration of the core and pair interaction are expected to make $C^* > C$ in most cases and equation (30) is consistent with this expectation.

CHAPTER 3

MEASUREMENT OF LINE STRENGTH RATIOS

The apparatus and procedures employed in measuring line strength ratios of selected strong Cs II lines are described in this chapter. This first section of the chapter deals with the general layout of the equipment. The last two sections describe the Cs II lamp and the spectrographic and photometric techniques.

The equipment was assembled originally to study the interaction of dense, free plasma beams with dense vapors of neutral atoms. It had been hoped that quasiresonant charge exchange reactions in the beam clashing zone might generate laser action at vacuum ultraviolet wavelengths. A spectrograph was appended to this apparatus to monitor transitions in the visible and near ultraviolet spectral regions. Spectrograms from this instrument proved to be rich in Cs II lines and prompted the work described here.

Figure 1 displays all the major features of the apparatus. Near the center of the figure is shown the vacuum chamber containing the Cs II lamp. Typical operating pressures in this chamber were about $0.2 \mu\text{Torr}$. The valve and rails constitute the plasma source described in the next section. The Cs vapor source and its flash tube are indicated to the right of the plasma source in the path of the plasma beam. The beam clashing region lies in a 5 cm by 2 mm strip about 1 mm from the face of the Cs source. Both the 1 m grating spectrograph and the

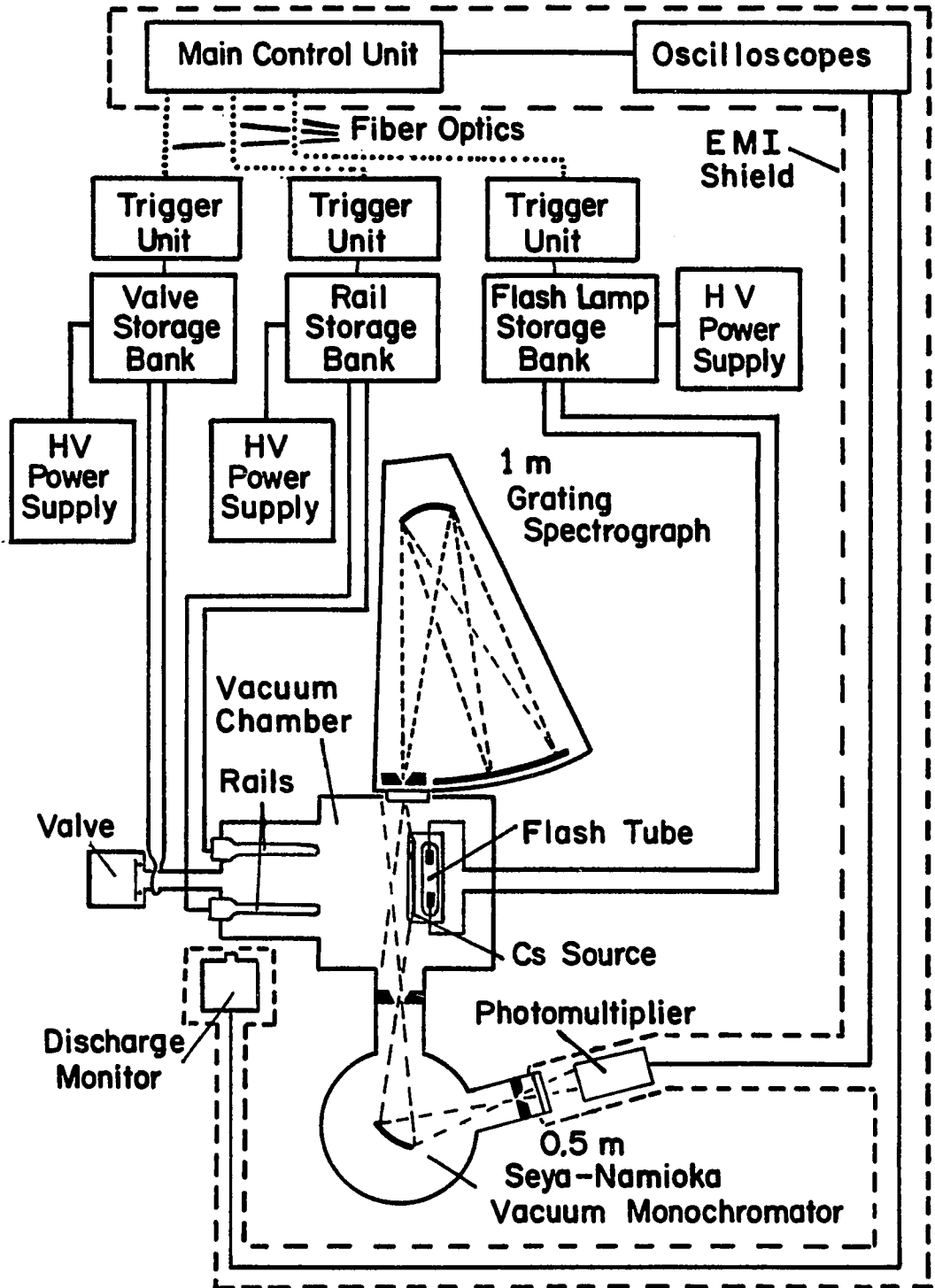


Figure 1. Schematic Diagram of Apparatus.

0.5 m Seya-Namioka vacuum monochromator have their optic axes along the long dimension of this strip.

The light passing into the 1 m spectrograph exits the vacuum chamber through a quartz window. There is a 2 mm by 5 mm aperture stop at this window to reduce the stray light from the flash tube and the plasma gun. The spectrograph entrance slit was adjusted to 40 μ by illuminating it with a collimated HeNe laser beam and observing the resultant diffraction pattern at the grating. The slit width was set so that the central maximum of the diffraction pattern just filled the 32 mm exposed width of the grating. For a fairly distant (17-22 cm) and localized (\sim 1 mm by 2 mm) source, this gives a nearly optimum combination of light gathering ability and spectral resolution.

The spectrograph grating has 600 grooves/mm and a 4000 Å blaze wavelength. It has good efficiency in the first order from about 2500 Å to about 6000 Å. The linear dispersion of the spectrograph averaged about 17 Å/mm at the Rowland circle film holder. The instrumental linewidth is measured to be 0.70 ± 0.04 Å. This linewidth is consistent with a value of 0.68 Å expected from the 40 μ slits with the spectrograph geometry. A mask near the film holder limits exposure of the film to a strip 4 mm by 26 cm. A vertical translation stage on the film holder allows seven separate strips to be exposed on the same sheet of film. The film and its processing are described at the end of this chapter.

The vacuum monochromator is open to the main vacuum chamber. It is equipped with a window at the exit slit. Monitoring the pulse to

pulse stability of various spectral lines from the Cs II lamp is its primary use in the present endeavor. The monochromator has a spherical concave grating. This grating is aluminized and has 600 grooves/mm. The 1500 Å blaze wavelength of this grating severely curtails the usefulness of the monochromator in the extreme vacuum ultraviolet, the efficiency being down theoretically to 15 percent of maximum at the He I resonance line, 584 Å. Three types of exit windows have been used to front the photomultiplier tube. These windows cover various spectral regions. For visible and near ultraviolet wavelengths, a quartz window was used. A pyrex window coated with a thin translucent phosphor layer provided broad band, if somewhat degraded, response from the visible to the extreme vacuum ultraviolet. A fast recovery phosphor, either sodium salicylate or p-terphenyl, was used. The third type of window was identical to the latter window except for the addition of an aluminum overcoating. This overcoating was approximately 1000 Å thick and fairly transparent from about 200 Å to about 700 Å. It blocks stray light at other wavelengths improving the signal to noise ratio in the extreme vacuum ultraviolet.

In all cases, the effluence of the monochromator was detected by a photomultiplier which is mounted in contact with the exit window. The photomultiplier has an S-11 photocathode response and a peak overall responsivity of 2000 Å/μm. The photomultiplier output is coupled through a shielded coaxial cable to a 180 MHz storage oscilloscope. A second 100 MHz storage oscilloscope displays the signal from the discharge monitor. The coupling here is also through a shielded coaxial

cable. The discharge monitor is a fast photodiode-opamp hybrid which is directed towards the plasma ignition region. It monitors the sequencing and relative performance of the various pulsed discharges.

These oscilloscopes, and the main control unit discussed below, reside within an electromagnetic interference (EMI) shield. This is a double Faraday cage fabricated from copper screen. Surrounding the two oscilloscopes and the main control unit with this shield proved necessary because of electromagnetic disturbances generated by the plasma gun and the Cs source.

As indicated in Figure 1, the main control unit controls the triggering of three separate high voltage discharges which are necessary to the operation of the Cs II lamp. The three discharges energize the valve, the rails and the flash tube. The three discharge circuits, shown in Figure 1, are quite similar to one another. Each has a trigger unit with a fiber optic receiver. In each trigger unit the receiver output drives a capacitive discharge circuit, transformer coupled to generate a high voltage trigger pulse. This trigger pulse is a 20-30 kV, high output impedance voltage pulse. Its duration is about 0.6 μ s. Each high voltage trigger pulse fires a triggered spark gap connected between a storage bank and the device it drives. The storage banks each consist of high voltage capacitors. These energy storage capacitors have low inductance and are designed for fast discharge applications. Separate high voltage power supplies charge each storage bank. The power supplies deliver 0-30 kV at 5.5 mA. The

details of each discharge circuit are discussed in the context of the device it drives.

For proper operation of the lamp, the sequencing of the three discharges must be timed to within a few microseconds. The main control unit accomplishes this with a dual delay generator operating from a 5 MHz crystal controlled clock. The output of the delay generator is in the form of an initial pulse followed by two delayed pulses. The delay times between the initial pulse and each delayed pulse are independently variable. Each output pulse feeds a separate fiber optic transmitter and appears as a light pulse from a high speed LED. Fiber optic cables carry the precisely timed light pulses through the EMI shield to fiber optic receivers on each of the trigger units. The receivers consist of photo-Darlington's connected to CMOS Schmitt triggers which were chosen for their high noise immunity. This method of trigger coupling minimizes the electrical noise inside the EMI shield. The main control unit also provides an electrical output pulse about 40 μ s prior to the first light pulse. This pulse is used to trigger the two oscilloscopes. Each oscilloscope has a delayed sweep time base permitting independent monitoring of the timing sequence.

The Cs II Lamp

The components discussed thus far control, energize and monitor the operation of the Cs II lamp. The lamp itself is comprised of a pulsed high density Cs source and a pulsed high density plasma source. The plasma source consists of a fast pulsed gas valve and a Marshall-type parallel rail plasma gun. The details of these components are set

forth in this section. First, however, it seems appropriate to discuss the basic operation of the Cs II lamp. Central to this discussion are the details of the timing sequence mentioned above.

The Cs II lamp operates in an electrodeless beam clashing mode. A hot, dense plasma pulse is ignited near the base of the rails and accelerates towards the Cs source (see Figure 1). This pulse is literally shot from the plasma gun and propagates freely across the vacuum chamber. The Cs source, meanwhile, has generated a pulse of atomic Cs vapor in the path of the plasma pulse. The Cs vapor is cool and dense. Suddenly, the two beams clash resulting in the violent ionization and excitation of the Cs atoms. There is a corresponding rapid cooling of the plasma. The burst of light from the interaction region where the collision takes place is typically rich in spectral lines of Cs II and of various species present in the plasma. In the present work He, Ar and H plasmas were used.

The location of the interaction region is determined by the delay time between establishing the Cs vapor beam and firing the plasma gun into it. Once the fields of view of the spectral instruments are set, a time sequence must be found which will place the interaction region within view. In actual operation, the first event is always the pulsing of the gas valve. When this pulse of gas reaches the region between the rails, the rails must be fired. Thus, the valve trigger to rail ignition delay time has a fixed value for each gas used in the plasma gun. On the basis of the photomultiplier signals for various spectral lines from the plasmas, the following valve-rail delay times

were judged qualitatively to produce optimum plasmas: He about 325 μs , Ar about 900 μs and H about 230 μs . As might be expected for gasses initially at the same temperature, the times are roughly in the same ratios as the roots of the molecular weights.

The same photomultiplier signals provide the time of flight of the plasma pulses. The flight times from ignition of the rails to arrival at the monochromator field of view were found to be 6 μs for He, 10 μs for Ar and 3 μs for H to an accuracy of about $\pm 0.5 \mu\text{s}$. Again, the He and H times are consistent with the difference in atomic weight and roughly equal effective kinetic temperatures. The flight time of the Ar plasma, however, is about half the anticipated value indicating an effective kinetic temperature some fourfold greater than the He and H plasmas. The cause of this appears to be the relatively greater amount of time that the Ar plasma spends in the acceleration region between the rails. This is consistent with the relatively greater atomic mass of Ar.

By summing the valve-rail delay time and the plasma flight time discussed above, the total delay time from the pulsing of the valve to the arrival of the plasma at the interaction region is found for each gas. It still remains to find the proper time at which to fire the Cs source flash tube so that the Cs pulse arrives at the interaction region simultaneous with the plasma pulse. Hot wire detector studies of the Cs source, which are discussed below, show by extrapolation that the maximum Cs vapor density lies just off the face of the Cs source about 25 μs prior to the arrival of the plasma pulse at the prescribed

interaction region. The corresponding valve trigger to flash tube trigger delay times are, therefore, about 306 μs for He, about 885 μs for Ar and about 208 μs for H. This establishes the overall timing sequences for proper operation of the Cs II lamp with plasmas of He, Ar and H.

Pulsed Gas Valve and Plasma Gun

Figure 2 shows a cross sectional view of the gas valve and plasma gun. The fast pulsed gas valve has a single moving part. This is the 25 mm (diameter) by 0.13 mm BeCu disk which has a mass of about 0.56 gm. Normally, the regulated 25 psig pressure of the gas in the reservoir keeps the disk pressed tightly against an o-ring. This o-ring has a 3/8" I.D. and a 1/16" thickness (values nominal). The disk seals on the o-ring and prevents gas in the reservoir from entering the vacuum chamber. When the valve is pulsed, the BeCu disk is inductively driven away from the o-ring. This allows gas from the reservoir to travel down the 7.1 mm bore of the valve neck and pour into the vacuum chamber midway between the rails. The energy for lifting the disk is supplied by discharging the 1.0 μF capacitor of the valve storage bank directly through a copper loop. This single turn of copper is coaxial with the disk and separated from it by 2 mm. It is fashioned from a length of 3 mm square copper bar and has a 21 mm I.D. The loop is firmly potted into the material of the valve neck to insure mechanical and electrical integrity. Typically, 25 kV is employed on the valve capacitor. Analysis of the underdamped current pulse through the copper loop indicates a peak current on the order of 20 kA.

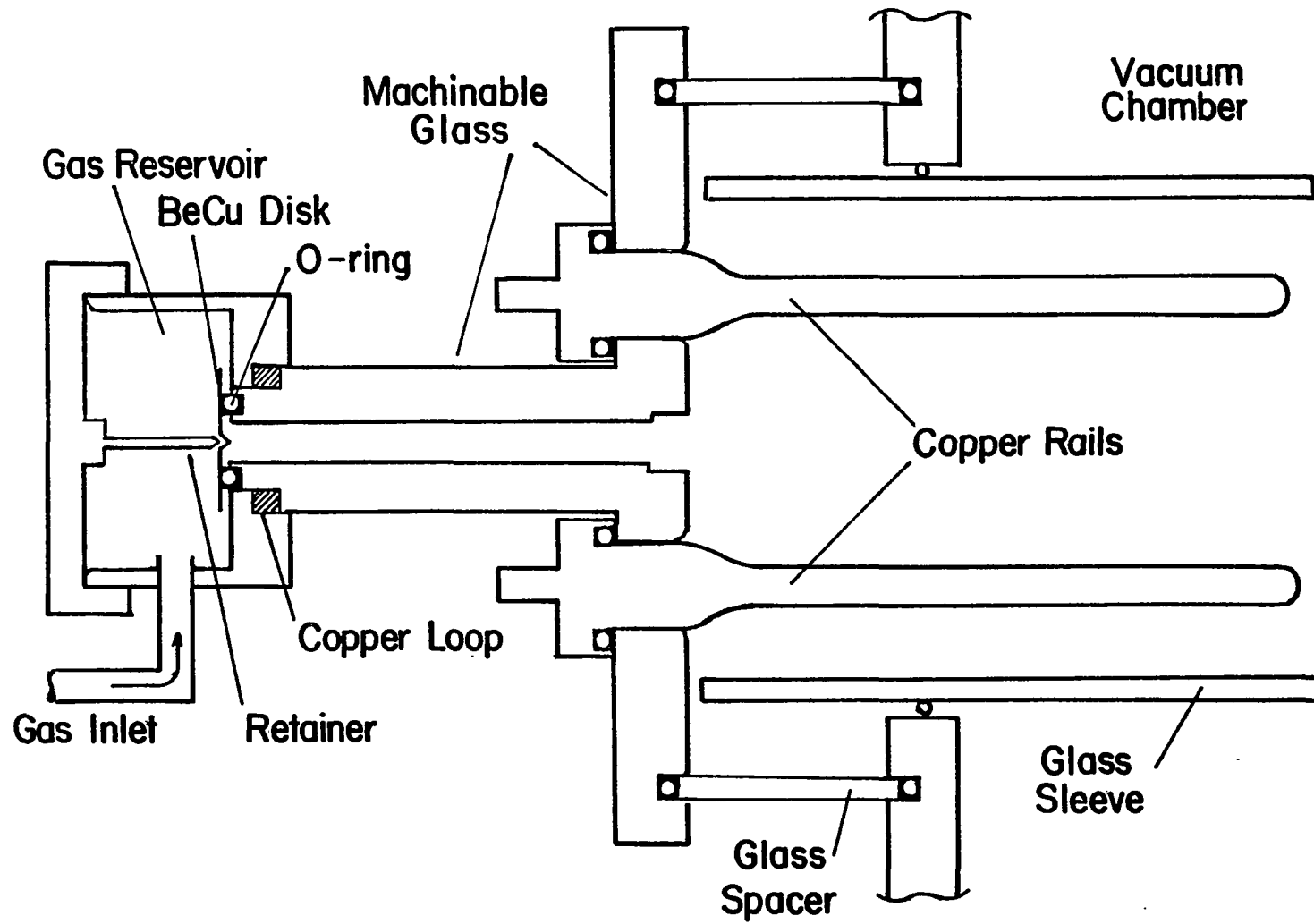


Figure 2. Diagram of Pulsed Gas Valve and Plasma Gun.

This data also shows a net series inductance of about $0.8 \mu\text{H}$ and a net series resistance of about $60 \text{ m}\Omega$ for the circuit. As the current pulse decays, the magnetic repulsion between the rapidly varying current in the loop and the corresponding induced currents in the disk weakens. This allows gas pressure in the reservoir and the spring loaded re-tainer to push the disk back against the o-ring. By this action, the vacuum seal is reinstated.

The valve neck and the flange holding the rails in place are made from Macor (Corning Glass Works, Inc.). This is a fluorophlogopite ($\text{KMg}_3\text{AlSi}_3\text{O}_{10}\text{F}_2$) based machinable glass-ceramic. It was chosen for its high mechanical and dielectric strengths and the ease with which it may be worked. Its performance in these regards is admirable. Macor proved, however, to have the undesirable property of shedding impurities into the plasma. Apparently, this is due to mica crystals in the microstructure which cleave away from the surface. Spectral lines of Mg, Si, F and B appear in the spectrograms as a result of this contamination from the Macor. Although boron is not included in the chemical formula above, it is a component of the final product.

The copper rails are mounted by means of threaded holes in the machinable glass flange. Their parallel axes are 51 mm apart. The rails extend 101 mm from the flange and are 6.8 mm in diameter over most of their length. The bases of the rails flare out over the 11 mm closest to the flange to a maximum diameter of 12 mm. The flaring further reduces the inductance near the base of the rails in an effort to encourage the plasma to ignite as close to the flange as possible.

The breakdown position is also somewhat dependent on the pressure distribution in the region between the rails. Thus, proper ignition of the rails partially depends on the valve parameters and the valve-rail delay time. For the timing sequence discussed above, the present configuration works reliably.

The rails are energized by the 0.5 μF capacitor of the rail storage bank. The capacitor voltage, typically 25 kV, is suddenly switched across the rails by triggering a spark gap. This ignites a low impedance arc between the rails at the low inductance end. The resultant abrupt change in current generates a rapidly rising magnetic flux which drives the plasma down the rails. Under optimum conditions, the plasma accelerates along the entire length of the rails. At the tips of the rails, it has sufficient momentum to propagate freely towards the Cs source. The net series inductance of the rail circuit is estimated to be on the order of 0.3 μH , and the net series resistance is on the order of 0.05 Ω . The peak current is probably around 10 kA. The formation of the plasma is a complex dynamic process. This and its transient nature make precise specification of circuit parameters unwarranted.

When operating the plasma gun with He or Ar gas, the addition of 5 vol % of H_2 insures prompt, reliable ignition of the plasmas. The hydrogen also provides a convenient means of measuring the electron density in each plasma. It so happens that the spectral line H_β , 4861 \AA , appears strongly in all the spectrograms. This line is dramatically Stark broadened in all the plasmas considered here.

Griem (1964, p. 305) gives the relationship,

$$N = C_{\lambda}(N,T)\Delta\lambda^{3/2}, \quad (31)$$

between the electron density N and the Stark width (FWHM) $\Delta\lambda$ of a spectral line λ . The coefficients C_{λ} depend only weakly on the electron density and the temperature T . These coefficients have been tabulated for a number of spectral lines including H_{β} (Griem 1964, p. 538). Linewidths of H_{β} were measured from the spectrograms by the methods discussed at the end of this chapter. With equation (31), these widths indicate electron densities on the order of 10^{15} cm^{-3} for all three types of plasmas, He, Ar and H. On the basis of qualitative comparisons of line intensities, the temperatures of all three plasmas seem to be of the same order of magnitude also. Temperatures were measured for the He plasmas. This was accomplished by determining the intensity ratio of the He II line, 4686 Å, to the He I line, 5876 Å, from each spectrogram. Comparison of the ratios so obtained to the graph given by Griem (1964, p. 274) showing the temperature dependence of this ratio yields an average temperature of $3.6 \pm 0.2 \text{ eV}$.

The glass spacer shown in Figure 2 fixes the distance from the tips of the rails to the face of the Cs source. This distance is about 57 mm in the present device. The glass sleeve serves to partially confine the gas from the valve just prior to plasma ignition. The sleeve also helped to prevent cataclysmic arcing between the rails and metal parts in the vacuum chamber.

Cs Vapor Source

The pulsed high density Cs source used here is a slight modification of the device described fully by Anderson, Jones and McCullen (1977). Its description shall be brief and will stress primarily the modifications. Figure 3 is a schematic diagram of the Cs source. The flash tube and the slide are the main components of the Cs vapor source. When the flash tube is triggered, a substantial fraction of its irradiance exits through the 3 mm by 5 cm slit in the flash tube cavity. Most of this radiation passes through the glass microscope slide and is absorbed by a metallic coating on the face of the slide. The present device has a slide coated with a 1000 Å thick layer of Ta. This coating appears to be more durable than the Fe coatings which were used previously (Anderson et. al. 1977). The visible light energy absorbed by the refractory metal coating is transferred as heat to a coating of metallic Cs which it melts and evaporates. The Cs metal coating vaporizes very rapidly producing a dense pulse of neutral atomic Cs vapor at the surface of the source.

In order to repeat this process, the Ta surface must be recoated with Cs. This is accomplished by lowering the Cs oven and mask to the positions indicated by dashed lines in Figure 3. In the lowered position, the oven sprays Cs onto the Ta surface of the slide. The orifice of the oven is 1 mm by 5 cm and made up of closely packed hypodermic needles. The lateral extent of the Cs coating, and thus of the Cs source itself, is limited by the slit in the mask. It is roughly 2 mm by 5 cm. Typical Cs coatings are on the order of

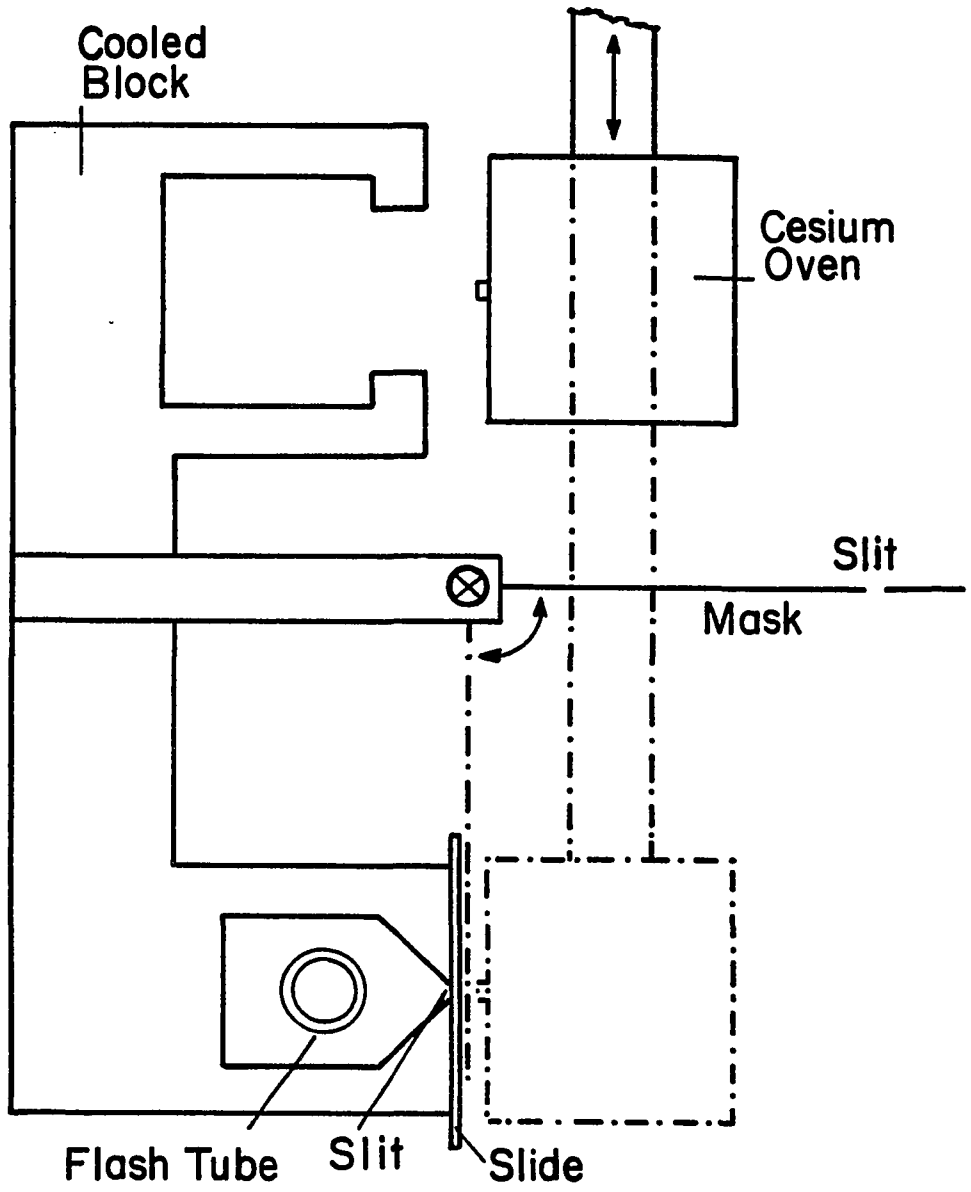


Figure 3. Diagram of Cs Vapor Source.

$10^{18} - 10^{17}$ atoms/cm². When not being used for coating, the Cs oven is in the raised position. In this position, the flux from the oven is trapped and condensed in a cavity in the cooled copper block.

A linear xenon flash tube is used on the present device. This tube is designed for long lifetime and high reliability under short pulse, high power excitation. The flash tube is driven by a 1.0 μ F capacitor in the flash tube storage bank (see Figure 1). Typical charging voltages are 12.5 kV to 13 kV corresponding to the stored energies of 78 J to 85 J. The current pulse has about 17 μ s total duration. The temporal characteristics of this pulse indicated a net series inductance of 0.91 μ H and a net series resistance of 0.37 Ω for the flash tube circuit. A peak current of about 10 kA follows from these circuit parameters.

A surface ionization hot wire detector is used to observe the Cs vapor pulses. Here, this detector consists of a white hot tungsten wire 25 μ m in diameter. This wire is mounted coaxially in a 1 cm diameter stainless steel collector. Cs vapor may pass through a 2 mm by 1 cm slit in the collector. This allows the hot wire to intercept and ionize a portion of the Cs flux. A bias voltage of 780 V accelerates the ionized Cs atoms from the hot wire to the collector. This yields a current which is proportional to the Cs flux.

The hot wire detector signals show the Cs source to have excellent pulse to pulse reproducibility. Measurements have been made at distances from the Cs source ranging from 2.5 cm to 7.0 cm. Arrival times for the peak of the pulse and for the leading and trailing half

maximum points of the pulse are very nearly linear in the distance. The slopes of these lines correspond to velocities of 620 m/s, 490 m/s and 450 m/s, respectively, for the leading half maximum, the peak and the trailing half maximum. If the arrival times are extrapolated to the face of the Cs source, then it is found that the leading half maximum leaves the slide about 22 μ s after the flash tube ignites. Similarly, the peak leaves about 25 μ s after ignition and the trailing half maximum leaves 60 μ s after ignition.

The normalized Cs pulse shape is described adequately by the expression (Anderson et. al. 1977),

$$J(\tau) = \exp[(1 - 1/\tau^2)^{5/2}]/\tau^5, \quad (32)$$

where J is the normalized flux and τ is the scaled time. The scaled time is related to the actual time t by

$$\tau = [t - (t_p - 1.232 \Delta t)]/(1.232 \Delta t), \quad (33)$$

where t_p is the actual peak arrival time and Δt is the pulse width (FWHM) in these same units. Both t and t_p are referred to an arbitrary origin. The quantity $(1.232 \Delta t)$ is the theoretical peak arrival time. Empirically, the peak arrival time is about $(2 \Delta t)$. This discrepancy is partially due to the assumption of a delta function initial pulse in formulating equation (32). This does not fully explain the discrepancy though and for this reason equation (32) should not be considered a rigorously valid model of the pulses described here. The pulse shape given by this expression does give an accurate fit to the observed pulses over the entire range of measurement given above, however, and serves as a useful tool in this regard.

Reasonably far from the Cs source, the peak flux is expected to fall off as $(1/z)^2$ where z is the distance from the source. This dependence follows from both radial spreading $(1/z)$ and the line source geometry $(1/z)$. For extremely small z , the source appears extended and only the radial spreading $(1/z)$ persists. The hot wire detector measurements show a $(1/z)^{1.6}$ dependence. If the peak Cs density near the source is to be estimated, then it seems clear that extrapolation of the measured dependence overestimates this density. On the other hand, the $(1/z)$ extrapolation from the measured points certainly underestimates it. Therefore, upper and lower bounds on the Cs density near the source may be found. At a distance of 1 mm from the face of the Cs source, the peak density is found to be between $2 \cdot 10^{15} \text{ cm}^{-3}$ and $1 \cdot 10^{16} \text{ cm}^{-3}$.

In the timing sequence discussed at the beginning of this section, the plasma arrives 1 mm from the slide 25 μs after the flash tube is triggered. At this time, the peak of the Cs pulse is just leaving the face of the source and the leading half maximum is 2 mm from it. This insures a high density and a steep density gradient for the Cs vapor in the interaction region.

Spectrographic and Photometric Techniques

All the spectrographic and photometric techniques employed in this research are fairly standard. The objective here is to develop a reliable means of measuring relative intensities on the spectrograms. This is necessary both for the plasma diagnostics discussed above and for the estimation of line strength ratios.

As mentioned at the beginning of this chapter, the spectrograph can make seven separate exposures on a single sheet of film. This allows a means of obtaining a relative exposure calibration on each sheet. In this procedure, the first strip on the film is exposed to one pulse from the Cs II lamp; the second strip is exposed to two pulses, the third to four pulses, and so on. Usually, the maximum exposure was 32 shots on the sixth strip with the seventh strip being left in reserve.

The spectrograms in the present work were taken on Kodak Tri-X Pan (TX-120) roll film. This film has a nominal speed of 400 ASA. Its spectral response is reasonably flat from about 2500 Å to about 6500 Å making it ideally suited to the present purpose. In order to reduce the exposure time, the film was developed in Beseler UltraFin FD7. This developer is designed to give the maximum effective film speed. It yields developed film with fine grain, good acutance and smooth tonality. The spectrograms were developed for 20 minutes with constant agitation in a rocking tray to achieve an effective speed of about 1600 ASA. Following development, the film was immersed in Kodak Indicator Stop Bath for 30 seconds, then fixed in Kodak Rapid Fixer for four minutes. Next, the film was washed in running water for one minute, soaked in Kodak Hypo Clearing Agent for two minutes and washed again in water for five minutes. Finally, the film is put into dilute Kodak Photo Flo solution for 30 seconds, then carefully sponged and hung to dry.

The processed film is analyzed on a scanning microdensitometer. By plotting the measured density against the logarithm of the exposure for a particular spectral line as it appears in different strips, the characteristic curve for the entire system is found. The unit of exposure used here is a single shot of the Cs II lamp. This generates a relative calibration only. Since the temporal characteristics of each unit of exposure are nearly the same, reciprocity effects are automatically included.

Figure 4 shows a plot of the film characteristics given by the above procedure. The upper curve shows a sequence of exposures for the He I spectral line 5876 Å. The lower trace is for the He II line 4686 Å as it appeared in the same spectrograms. The points marked on each curve correspond to exposures of 2, 4, 8 and 16 shots. The horizontal separation of the two curves gives the effective exposure ratio for these two spectral lines from the plasma. By correcting this ratio for the relative spectral sensitivity of the system (see the discussion following equation [34] below) at the two wavelengths, the line intensity ratio is found. From the graph, the intensity of the 4686 Å line relative to the 5876 Å line is 0.072. This ratio is used in measuring the temperature of the plasma as discussed in the preceding section.

The two curves in Figure 4 cover the entire linear range of the characteristic curve. This range is about five octaves of exposure. The slopes of the linear sections give an effective gamma of 0.644 for the photometric system. It follows that the relative intensity I corresponding to a measured transmittance T is given by

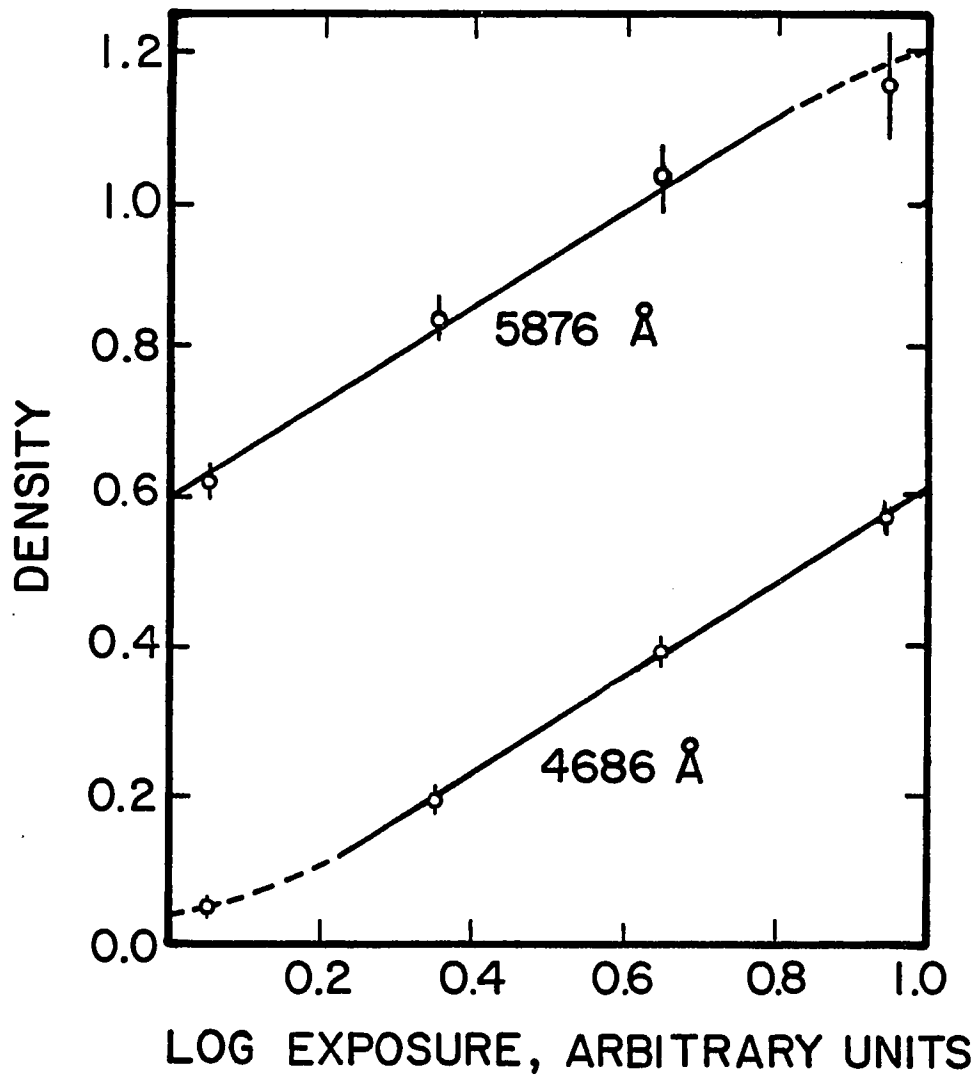


Figure 4. Plot of Film Characteristics.

$$I = 1/[\eta(\lambda)T^{1.55}], \quad (34)$$

where η is the relative spectral sensitivity of the overall system at the wavelength λ being considered. In this work, values of η were obtained by multiplying the efficiency predicted by the blaze equation for the grating by the relative spectral sensitivity of the film given by Kodak (1973, p. 19d).

Each spectrogram covered the spectral range from about 2700 Å to about 6300 Å. Strong, well-known lines were easily identified in every instance. Unknown wavelengths then could be identified by linear interpolation between the closest known lines. Usually, the identification could be made to an accuracy of about ± 0.05 Å. Wavelength separations as small as about 0.5 Å were discerned. The wavelength tables of Striganov and Sventitskii (1968) and of Harrison (1939) were used throughout this procedure. This ultimately led to the identification of 42 classified and 38 unclassified lines from Cs II in the spectrograms. No assigned lines from Cs I or Cs III appeared in the spectrograms. Numerous lines from the plasma and its impurities were observed in the spectrograms. One strong line, measured to be 5260.93 ± 0.11 Å in first order, appeared persistently in the spectrograms and eluded every attempt at identification.

CHAPTER 4

RESULTS AND CONCLUSIONS

This chapter analyzes Cs II from the perspective of the research described above. The first section of the chapter applies the theoretical results of Chapter 2 to the spectrum of Cs II. Calculated line strengths, as given by the ECP approximation, are tabulated for all the transitions, 5d,6s-6p and 6p-6d,7s. In the second section, line strength ratios derived from the calculated values are compared with measured ratios. The observed line strength ratios are measured by the method of Chapter 3. In this section, two other types of calculated ratios also are compared to the observed values. These are obtained from the Coulomb approximation and a least squares fitting procedure. The third and final section contains conclusions drawn from the present work and some suggestions for further development.

Calculated Cs II Line Strengths

The line strengths which are tabulated in this section were calculated in the ECP approximation. Singly excited Cs II has a $[\text{Kr}]4d^{10} 5s^2 5p^5 n\ell$ configuration. This system may be approximated as a single optical electron bound to a static core for transitions not involving the ground state. The ground state transitions all have wavelengths deep in the vacuum ultraviolet (Reader and Epstein 1975) and are not considered here. Throughout the following, the fixed core

configuration is not explicitly written, but is implicitly as shown above. The excited states of Cs II are specified by their configuration, $n\ell$, and their $J_1\ell$ term values, $J_1[K]_J$. The angular momentum coupling here is $|\gamma, n\ell; [[L_1 S_1] J_1\ell] K_{\frac{1}{2}} JM\rangle$. These states are an inadequate description of Cs II and serve primarily as a convenient nomenclature.

By utilizing a multiconfigurational Hartree-Fock procedure, Reader (1976) calculated composition amplitudes for many energy levels in Cs II. These amplitudes produce a good fit to the empirical energy levels. Reader also clarifies the Cs II energy level structure in this work. The amplitudes from the Hartree-Fock procedure are given in the LS basis and are of the type considered in equation (6). As considered here, the Cs II system may be analyzed in the manner of the example in Chapter 2. The C coefficients in the line strength expansion are as shown in equation (7). The amplitudes supplied by Reader (1976), however, are evaluated in a different phase convention than that used in the derivation of equation (7). Therefore, it is necessary to adjust their phases. The phase factors required for this adjustment were found by comparing amplitudes supplied by Reader (1978) for the diagonal transformation $J_1\ell - LS$ with the corresponding diagonal amplitudes for the present conventions. It should be noted that the phases given by Reader (1976) are also internally inconsistent: the 6p configuration is calculated with a different phase convention than the 5d,6s and 6d,7s configurations.

TABLE I. Cs II Line Strengths: $5d, 6s \frac{1}{2} [K]_J - 6p \frac{1}{2} [K']_{J'}$

Configuration	Term Energy	6p			
		$\frac{1}{2} [1\frac{1}{2}]_0$ 144 532	$\frac{1}{2} [1\frac{1}{2}]_1$ 143 361	$\frac{1}{2} [1\frac{1}{2}]_1$ 141 564	$\frac{1}{2} [1\frac{1}{2}]_2$ 143 403
5d	$\frac{1}{2} [1\frac{1}{2}]_1^0$ 139 249	(18 927) 3.76	(24 319) 1.00	(43 187) 1.63	(24 073) 0.152
	$\frac{1}{2} [1\frac{1}{2}]_2^0$ 128 320 ^a		6646.56 ^b 13.3	(7548) 0.0780	6627.77 ^b 1.87
	$\frac{1}{2} [2\frac{1}{2}]_2^0$ 126 697 ^a		(5999) 0.596	6724.48 ^b 12.8	5984.39 ^b 1.78
	$\frac{1}{2} [2\frac{1}{2}]_3^0$ 129 420 ^a				7149.55 ^b 21.4
6s	$\frac{1}{2} [1\frac{1}{2}]_0^0$ 122 374		4763.62 60.8	5209.62 38.9	
	$\frac{1}{2} [1\frac{1}{2}]_1^0$ 122 875	4616.13 23.3	4879.95 35.6	5349.16 55.7	4870.02 136

^aNew level, see Appendix A.^bNew classification, see Appendix A.

TABLE II. Cs II Line Strengths: $5d, 6s \frac{1}{2} [K]_J - 6p \frac{1}{2} [K']_J$.

Configuration	Term	6p					
		$\frac{1}{2} [^2\frac{1}{2}]_0$	$\frac{1}{2} [^2\frac{1}{2}]_1$	$\frac{1}{2} [^2\frac{1}{2}]_1$	$\frac{1}{2} [^2\frac{1}{2}]_2$	$\frac{1}{2} [^2\frac{1}{2}]_2$	$\frac{1}{2} [^2\frac{1}{2}]_3$
	Energy	133 162	126 527	129 999	130 775	128 099	129 117
5d	$\frac{1}{2} [^2\frac{1}{2}]_1^0$	(16 430)	(7859)	(10 810)	(11 801)	(8966)	
	139 249	1.46	0.0232	1.27	0.0642	0.0468	
	$\frac{1}{2} [^2\frac{1}{2}]_2^0$		(55 796)	(59 561)	(40 730)	(5·10 ⁵)	(1·10 ⁵)
	128 320 ^a		0.521	0.0405	0.0788	0.0234	1.19
	$\frac{1}{2} [^2\frac{1}{2}]_2^0$		(6·10 ⁵)	(30 290)	(24 523)	(71 349)	(41 333)
	126 697 ^a		0.013	0.276	0.00286	0.229	0.0116
$\frac{1}{2} [^2\frac{1}{2}]_3^0$				(73 807)	(75 684)	(3·10 ⁵)	
129 420 ^a				0.00262	0.397	0.168	
6s	$\frac{1}{2} [^2\frac{1}{2}]_0^0$		(24 079)	(13 116)			
	122 374		0.334	0.0470			
	$\frac{1}{2} [^2\frac{1}{2}]_1^0$	(9718)	(27 378)	(14 038)	(12 658)	(19 143)	
122 875	0.114	0.199	0.510	0.539	0.297		

^aNew level, see Appendix A.

TABLE III. Cs II Line Strengths: $5d, 6s \frac{1}{2} [K]_J - 6p \frac{1}{2} [K']_J$

Configuration	6p					
	Term Energy	$\frac{1}{2} [1/2]_0$ 144 532	$\frac{1}{2} [1/2]_1$ 143 361	$\frac{1}{2} [1/2]_1$ 141 564	$\frac{1}{2} [1/2]_2$ 143 403	
5d	$1\frac{1}{2} [1/2]_0^0$ 107 572		2793.32 1.07	2940.95 1.09		
	$1\frac{1}{2} [1/2]_1^0$ 107 914	2730.06 0.00272	2820.27 0.243	2970.85 0.636	2816.94 2.52	
	$1\frac{1}{2} [1\frac{1}{2}]_1^0$ 123 645	4786.36 12.0	5070.68 3.57	5579.03 6.18	5059.87 32.2	
	$1\frac{1}{2} [1\frac{1}{2}]_2^0$ 112 804		3271.63 1.29	3475.97 $94 \cdot 10^{-6}$	3267.14 0.561	
	$1\frac{1}{2} [2\frac{1}{2}]_2^0$ 115 675 ^a		3610.86 ^b 0.011	3861.49 ^b 0.441	3605.54 ^b 0.0740	
	$1\frac{1}{2} [2\frac{1}{2}]_3^0$ 118 269 ^a				3977.53 ^b 0.00346	
	$1\frac{1}{2} [3\frac{1}{2}]_3^0$ 113 726				3368.56 0.544	
	$1\frac{1}{2} [3\frac{1}{2}]_4^0$ 112 245					
	6s	$1\frac{1}{2} [1\frac{1}{2}]_1^0$ 110 954	2977.26 0.398	3084.88 0.255	3265.92 0.988	3080.87 0.174
		$1\frac{1}{2} [1\frac{1}{2}]_2^0$ 107 401		2780.06 0.495	2926.27 0.0163	2776.99 0.0841

^aNew level, see Appendix A.^bNew classification, see Appendix A.

TABLE IV. Cs II Line Strengths: $5d,6s\ 1\frac{1}{2}[K]_J - 6p\ 1\frac{1}{2}[K']_{J'}$

Configuration	6p						
	Term	$1\frac{1}{2}[1\frac{1}{2}]_0$	$1\frac{1}{2}[1\frac{1}{2}]_1$	$1\frac{1}{2}[1\frac{1}{2}]_1$	$1\frac{1}{2}[1\frac{1}{2}]_2$	$1\frac{1}{2}[2\frac{1}{2}]_2$	$1\frac{1}{2}[2\frac{1}{2}]_3$
Energy	133 162	126 527	129 999	130 775	128 099	129 117	
5d	$1\frac{1}{2}[1\frac{1}{2}]_0^0$		5274.04	4457.68			
	107 572		3.38	0.144			
	$1\frac{1}{2}[1\frac{1}{2}]_1^0$	3959.50	5370.98	4526.72	4373.02	4952.84	
	107 914	11.1	11.0	38.7	16.0	50.9	
	$1\frac{1}{2}[1\frac{1}{2}]_1^0$	(10 507)	(34 697)	(15 740)	(14 026)	(22 455)	
	123 645	4.17	0.341	1.62	0.0777	0.372	
	$1\frac{1}{2}[1\frac{1}{2}]_2^0$		(7285)	5814.18	5563.02	6536.44	6128.62
	112 804		3.78	3.44	43.8	16.7	31.8
	$1\frac{1}{2}[2\frac{1}{2}]_2^0$		(9212)	6979.68 ^b	(6621)	(8047)	(7438)
	115 675 ^a		0.570	10.1	0.0254	4.05	0.734
	$1\frac{1}{2}[2\frac{1}{2}]_3^0$				(7994)	(10 173)	(9216)
	118 269 ^a				17.2	1.59	3.14
	$1\frac{1}{2}[3\frac{1}{2}]_3^0$				5863.70	6955.52	6495.53
	113 726				0.176	17.2	4.02
$1\frac{1}{2}[3\frac{1}{2}]_4^0$						5925.65	
112 245						28.2	
6s	$1\frac{1}{2}[1\frac{1}{2}]_1^0$	4501.52	6419.54	5249.37	5043.80	5831.16	
	110 954	22.8	0.0407	60.5	49.4	56.4	
	$1\frac{1}{2}[1\frac{1}{2}]_2^0$		5227.00	4424.05	4277.10	4830.16	4603.76
107 401		98.1	1.47	69.8	48.9	207	

^aNew level, see Appendix A.^bNew classification, see Appendix A.

TABLE V. Cs II Line Strengths: $6p \frac{1}{2}[K]_J - 6d, 7s \frac{1}{2}[K']_J$

Configuration	Term Energy	6p			
		$\frac{1}{2}[^2_2]_0$ 144 532	$\frac{1}{2}[^2_2]_1$ 143 361	$\frac{1}{2}[^2_2]_1$ 141 564	$\frac{1}{2}[^2_2]_2$ 143 403
6d	$\frac{1}{2}[^2_2]_1^0$ 169 192	4053.96 50.4	3870.16 14.5	3618.55 22.9	(3876) 2.40
	$\frac{1}{2}[^2_2]_2^0$ 166 970		4234.41 133	(3935) 0.0123	4241.97 16.7
	$\frac{1}{2}[^2_2]_2^0$ 166 696		4284.23 2.37	3978.00 128	4292.01 20.9
	$\frac{1}{2}[^2_2]_3^0$ 167 025				4232.19 212
	$\frac{1}{2}[^2_2]_0^0$ 163 034		5081.77 0.0509	4656.54 0.0511	
	$\frac{1}{2}[^2_2]_1^0$ 163 189	5358.53 0.0336	5041.83 0.0366	4623.09 0.0846	5052.70 0.182
7s					

TABLE VI. Cs II Line Strengths: $6p \frac{1}{2}[K]_J - 6d, 7s \frac{1}{2}[K']_J$,

Configuration	6p				
	Term	$\frac{1}{2}[\frac{1}{2}]_0$	$\frac{1}{2}[\frac{1}{2}]_1$	$\frac{1}{2}[1\frac{1}{2}]_1$	$\frac{1}{2}[1\frac{1}{2}]_2$
Energy	144 532	143 361	141 564	143 403	
6d	$1\frac{1}{2}[\frac{1}{2}]_0^0$		(12 017)	(9881)	
	151 682		0.522	0.00695	
	$1\frac{1}{2}[\frac{1}{2}]_1^0$	(13 074)	(11 338)	(9417)	(11 392)
	152 181	0.0736	0.773	0.00156	0.119
	$1\frac{1}{2}[1\frac{1}{2}]_1^0$	(8418)	(7662)	(6735)	(7687)
	156 408	0.177	0.355	0.251	0.0855
	$1\frac{1}{2}[1\frac{1}{2}]_2^0$		(10 594)	(8898)	(10 641)
	152 800		0.154	0.184	0.434
	$1\frac{1}{2}[2\frac{1}{2}]_2^0$		(10 050)	(8511)	(10 093)
	153 311		0.00857	0.0699	0.00700
	$1\frac{1}{2}[2\frac{1}{2}]_3^0$				(9721)
	153 687				0.0483
$1\frac{1}{2}[3\frac{1}{2}]_3^0$				(10 591)	
152 845				0.00072	
$1\frac{1}{2}[3\frac{1}{2}]_4^0$					
152 558					
7s	$1\frac{1}{2}[1\frac{1}{2}]_1^0$	(19 678)	(15 992)	(12 423)	(16 100)
	149 614	0.0203	0.00384	0.0124	0.00665
	$1\frac{1}{2}[1\frac{1}{2}]_2^0$		(17 064)	(13 061)	(17 188)
	149 221		0.0949	$56 \cdot 10^{-6}$	0.0740

TABLE VII. Cs II Line Strengths: $6p\ 1\frac{1}{2}[K]_J - 6d,7s\ \frac{1}{2}[K']_J$

Configuration	6p						
	Term	$1\frac{1}{2}[^2]_0$	$1\frac{1}{2}[^2]_1$	$1\frac{1}{2}[^1\frac{1}{2}]_1$	$1\frac{1}{2}[^1\frac{1}{2}]_2$	$1\frac{1}{2}[^2\frac{1}{2}]_2$	$1\frac{1}{2}[^2\frac{1}{2}]_3$
Energy	133 162	126 527	129 999	130 775	128 099	129 117	
6d	$\frac{1}{2}[^1\frac{1}{2}]_1^0$	(2775)	2343.13	2550.65	(2602)	2432.71	
	169 192	0.199	0.0287	0.561	0.144	0.0126	
	$\frac{1}{2}[^1\frac{1}{2}]_2^0$		2471.88	2703.95	2761.97	2571.79	2640.92
	166 970		1.23	0.00066	0.470	0.119	0.0270
	$\frac{1}{2}[^2\frac{1}{2}]_2^0$		2488.74	2724.21	(2783)	2590.09	2660.24
	166 696		0.0294	0.159	0.0421	0.00445	0.00141
$\frac{1}{2}[^2\frac{1}{2}]_3^0$				2757.81	2568.17	2637.14	
167 025				0.151	0.00607	0.0747	
7s	$\frac{1}{2}[^2]_0^0$		(2738)	(3026)			
	163 034		0.152	0.00649			
	$\frac{1}{2}[^2]_1^0$	3329.43	2726.80	3012.04	(3084)	2848.96	
163 189	0.119	0.220	0.0679	0.0581	0.00632		

TABLE VIII. Cs II Line Strengths: $6p\ 1\frac{1}{2}[K]_J - 6d,7s\ 1\frac{1}{2}[K']_J$

Configuration	6p						
	Term	$1\frac{1}{2}[1\frac{1}{2}]_0$	$1\frac{1}{2}[1\frac{1}{2}]_1$	$1\frac{1}{2}[1\frac{1}{2}]_1$	$1\frac{1}{2}[1\frac{1}{2}]_2$	$1\frac{1}{2}[2\frac{1}{2}]_2$	$1\frac{1}{2}[2\frac{1}{2}]_3$
Energy	133 162	126 527	129 999	130 775	128 099	129 117	
6d	$1\frac{1}{2}[1\frac{1}{2}]_0^0$		3974.24	4610.50			
	151 682		28.6	1.11			
	$1\frac{1}{2}[1\frac{1}{2}]_1^0$	5256.57	3896.98	4506.83	4670.28	4151.27	
	152 181	0.765	64.8	0.562	14.1	7.61	
	$1\frac{1}{2}[1\frac{1}{2}]_1^0$	4300.64	(3346)	3785.42	3900.09	3531.38	
	156 408	49.6	0.0364	37.7	0.200	2.62	
	$1\frac{1}{2}[1\frac{1}{2}]_2^0$		3805.10	4384.43	4538.94	4047.18	4221.12
	152 800		53.2	10.6	66.4	8.80	8.46
	$1\frac{1}{2}[2\frac{1}{2}]_2^0$		3732.54	4288.35	4436.06	3965.19	4132.00
	153 311		1.73	100	0.0161	47.7	1.92
	$1\frac{1}{2}[2\frac{1}{2}]_3^0$				4363.28	3906.93	4068.77
	153 687				168	10.4	34.2
	$1\frac{1}{2}[3\frac{1}{2}]_3^0$				(4530)	4039.84	4213.13
	152 845				0.325	176	36.7
$1\frac{1}{2}[3\frac{1}{2}]_4^0$						4264.68	
152 558						273	
7s	$1\frac{1}{2}[1\frac{1}{2}]_1^0$	6076.74	4330.24	5096.60	5306.61	4646.51	
	149 614	0.0484	1.42	0.336	0.731	0.00908	
	$1\frac{1}{2}[1\frac{1}{2}]_2^0$		4405.25	(5201)	5419.69	4732.98	4972.59
	149 221		0.693	0.606	2.73	0.387	0.0118

are in the infrared and the far infrared regions of the spectrum where spectroscopic data is sadly lacking for Cs II.

The row and column headings in the tables give the designations and energies of the levels. As discussed above, the designations are only nominal. The level energies are in cm^{-1} and each is given directly below the nominal term corresponding to it. The energies are either from Reader (1976) or Appendix A. Each nominal designation is assigned according to the dominant amplitude in the composition of the level. Blank entries in the tables indicate forbidden transitions for which the line strength vanishes.

Comparison of Observed and Calculated Ratios

The observed line strength ratios are obtained from the measured relative line intensities of equation (34). The relevant expression for the line strength ratio follows from the definition of the line intensity (Condon and Shortley 1970, p. 98) and is written as

$$S(E_i, E_f)/S(E'_i, E'_f) = \lambda^4 N'_i I / (\lambda'^4 N_i I'), \quad (35)$$

where λ and I are, respectively, the wavelength and relative line intensity of the transition $E_i \rightarrow E_f$, and where λ' and I' are the corresponding quantities for the transition $E'_i \rightarrow E'_f$. In equation (35), N_i and N'_i are the respective population numbers of the initial levels E_i and E'_i . The accurate estimation of level populations is very difficult. This is especially true in the present instance because it probably is not valid to assume a thermal equilibrium population distribution for the source described in Chapter 3. The temperature of this

source is a dynamic quantity which varies rapidly at the time of peak light emission. Thus, it is convenient to present the experimental data from the present work in the form of line strength ratios for lines with a common upper level. For these ratios, the population factors in equation (35) cancel and the result is independent of the mode and extent of excitation.

Table IX displays all the Cs II line strength ratios which could be obtained from the present spectrograms in this fashion. The analysis of each spectrogram led to a value for each of the ratios. The values so obtained from a number of spectrograms were averaged to yield the observed ratios shown in the table. In most cases, the uncertainty associated with a particular ratio was taken to be the standard deviation of the measured values from the average. Whenever the standard deviation was less than the uncertainty indicated by propagation of errors, however, the latter value was chosen instead.

For each upper level shown in Table IX, all possible ratios are given in order of decreasing magnitude. All possible ratios were taken to avoid biasing the tabulated ratios by the choice of any one particular value as a normalization factor. This leads, however, to an effective multiple counting of some of the data. Care was taken to compensate for this in the statistical analysis described below.

The first column of Table IX gives the nominal designation of the upper levels. This is followed in columns two and three by the wavelengths corresponding respectively to the line strengths of the numerator and denominator of the ratio being considered. The observed

TABLE IX. Comparison of Observed and Calculated Line Strength Ratios in Cs II

Upper Level	λ		Observed Ratio	Calculated Ratios		
	Numer.	Denom.		Fitted	ECP	Coulomb
6p $\frac{1}{2}$ [$\frac{1}{2}$] ₀	4616.1	4786.4	0.426±0.064	0.895	1.94	409
6p $\frac{1}{2}$ [$\frac{1}{2}$] ₀	3959.5	4501.5	0.248±0.032	0.325	0.486	1.33
6p $\frac{1}{2}$ [$\frac{3}{2}$] ₁	5274.0	5371.0	0.429±0.124	0.451	0.298	1.52
	5371.0	5227.0	0.127±0.025	0.250	0.112	0.138
	5274.0	5227.0	0.058±0.023	0.113	0.034	0.210
6p $\frac{1}{2}$ [$\frac{3}{2}$] ₁	5249.4	4526.4	0.790±0.119	1.63	1.56	1.39
6p $\frac{1}{2}$ [$\frac{5}{2}$] ₂	5563.0	4277.1	0.617±0.093	1.58	0.628	0.001
	4373.0	5043.8	0.262±0.039	0.146	0.324	2.04
	5043.8	5563.0	0.256±0.084	0.741	1.13	210
	5043.8	4277.1	0.160±0.051	1.17	0.708	0.174
	4373.0	5563.0	0.066±0.012	0.108	0.366	429
	4373.0	4277.1	0.040±0.007	0.170	0.230	0.356
6p $\frac{1}{2}$ [$\frac{5}{2}$] ₂	4830.2	4952.8	0.846±0.169	0.734	0.960	2.20
	4952.8	5831.2	0.852±0.170	1.26	0.903	0.338
	4830.2	5831.2	0.721±0.108	0.928	0.866	0.744
6p $\frac{1}{2}$ [$\frac{7}{2}$] ₃	5925.6	4603.8	0.563±0.135	0.560	0.136	0.617
6d $\frac{1}{2}$ [$\frac{1}{2}$] ₁ ⁰	3785.4	4300.6	0.434±0.065	0.758	0.760	0.720
6d $\frac{1}{2}$ [$\frac{3}{2}$] ₂ ⁰	3805.1	4538.9	0.491±0.074	0.823	0.801	1.27
6d $\frac{1}{2}$ [$\frac{5}{2}$] ₂ ⁰	3965.2	4288.4	0.239±0.057	0.476	0.475	0.488
6d $\frac{1}{2}$ [$\frac{7}{2}$] ₃ ⁰	4068.8	4363.3	0.096±0.033	0.203	0.203	0.203
6d $\frac{1}{2}$ [$\frac{9}{2}$] ₃ ⁰	4213.1	4039.8	0.087±0.022	0.209	0.209	0.209
7s $\frac{1}{2}$ [$\frac{1}{2}$] ₂ ⁰	4405.2	4972.6	0.701±0.070	0.704	58.8	0.282
Correlation Coefficients ^a				+0.85	+0.71	-0.013
$\langle 6s d 6p \rangle / \langle 5d d 6p \rangle$				-2.76	-5.72	+2.89
$\langle 6p d 7s \rangle / \langle 6p d 6d \rangle$				+0.0556	+0.0286	-0.481

^aThe level 7s $\frac{1}{2}$ [$\frac{1}{2}$]₂⁰ is not included; see text.

line strength ratios and their uncertainties appear in the fourth column. The last three columns of the table give three types of calculated ratios. Column five gives ratios calculated from a least squares fit to the observed ratios which is explained in the next paragraph. The sixth column contains the line strength ratios obtained from the ECP values given in Tables I through VIII of this work. The last column in Table IX gives line strength ratios calculated in the Coulomb approximation. The method of evaluation here is the same as for the ECP values except that the radial integrals are obtained from the Bates-Damgaard tables (Bates and Damgaard 1949, pp. 120-24; Sobel'man 1972, pp. 344-49).

The least squares fit mentioned above is based on the fact that for the configuration mixing considered here only two nonvanishing terms appear in each line strength expansion like equation (5). This means that each line strength ratio is a function of single parameter, namely, the ratio of the appropriate reduced matrix elements. Therefore, this latter ratio was treated as a free parameter and a least squares fit to the observed line strength ratios was performed. The reduced matrix element ratios obtained from this fitting procedure are shown in the last two rows of Table IX. For comparison, the corresponding ratios are given for the other two methods of calculation also.

The linear correlation coefficients between the observed line strength ratios and each column of calculated values have been computed. They appear in their respective columns just below the main body of the table. As indicated in the footnote to this entry in Table IX, the

ratio stemming from the $7s\ 1\frac{1}{2}[1\frac{1}{2}]_2^0$ level is excluded from the correlation analysis for all three columns. This was done because this ratio is extremely sensitive to very slight variations in the reduced matrix element ratio or in the C coefficients for the transition at 4972.6 Å. It is believed that the anomalous ECP value for this ratio is mostly a reflection of this sensitivity. This is supported by the fact that the fitted value for the 6p-6d,7s reduced matrix element ratio is strongly dominated by this ratio because of its sensitivity. Yet comparison of this fitted reduced matrix element ratio with the corresponding ECP value shows that the two are not much different. Since exclusion of this one ratio does not alter appreciably the linear correlation coefficients of either the fitted values or the Coulomb approximation values, this is judged to be a reasonable manipulation.

The correlation coefficient for the observed and fitted line strength ratios is a good deal less than unity. This seems to be due primarily to the uncertainties of the observed ratios. It may also result in part from an inadequacy on the behalf of the Hartree-Fock amplitudes. The poor showing by the Coulomb approximation is evident from both its small, negative correlation coefficient and examination of the table. As mentioned in Chapter 2, the Coulomb approximation is not expected to apply in the multiconfigurational approximation. It is included here primarily to illustrate this point. Although the Coulomb approximation gives reduced matrix element ratios of about the right magnitude as compared to the other two pairs of values, it gives

ratios of opposite phase. This phase difference is the major cause of the poor agreement between the Coulomb approximation ratios and the observed ones.

In order to further assess the validity of the ECP approximation, line intensities derived from Tables I through VIII were compared to the intensity figures given in published line lists. Three line lists which are primary sources (Olthoff and Sawyer 1932, Balasse 1927, Sommer 1924) were chosen for this comparison. The intensity figures in these works are based on visual estimates of photographic darkening. Therefore, it is assumed that these intensity figures are on a logarithmic scale. To compensate for this, the logarithm of each intensity calculated here was used. Also, it is assumed that the excitation of all the levels in the published works was about equal so that level populations need not be considered. Linear correlation coefficients were computed for each comparison. The linear correlation coefficients are +0.58 for 84 lines from Olthoff and Sawyer (1932), +0.50 for 109 lines from Balasse (1927) and +0.61 for 96 lines from Sommer (1924). Considering the assumptions made above, these correlations are impressive. From all these results, it would appear that the ECP method is a crude and imperfect approximation, but it also seems clear that it may serve as a useful means of estimating relative line strengths.

Conclusions

This chapter has presented and compared calculated and observed relative line strengths for Cs II. That has been the goal of this dissertation. In obtaining these line strength ratios, novel experimental

and theoretical techniques have been employed. The ECP approximation method of estimating line strengths appears to be a reasonably useful procedure. More extensive testing is required, however, to fully ascertain its accuracy and reliability. Although the results of the ECP method agree favorably with observation, there are sufficient discrepancies to indicate the need for a more refined approximation of comparable simplicity which is applicable to multiconfigurational states. Another approach which is presently being developed consists of including the next term in the asymptotic expansion of the potential shown in equation (13) of Chapter 2. In this new approximation, the value of the coefficient of the $(1/r)$ term is determined by the behavior of the potential at infinity as in the Coulomb approximation. The coefficient of the second order term, $(1/r^2)$, then is chosen so as to make the radial function vanish at the origin and have the appropriate number of radial nodes $(n-l-1)$. This new procedure leads to radial wave functions which are similar to those of Bates and Damgaard (1949) and which also have the phases and desirable analytical properties of the ECP approximation.

The validity of the absolute line strength values has not been considered here. At this time, it is not known how well the ECP line strengths in Tables I through VIII agree with actual absolute line strengths. The values in the tables, therefore, should be regarded only as relative line strengths until they are examined in this regard.

In obtaining the measured line strength ratios, a novel lamp has been employed which operates in an electrodeless beam clashing

mode. With little modification, many metals may be used as the spectral source in this lamp. Probably all the alkali metals, and possibly other metals with low boiling points, such as Ba and Ca, may be employed. With the present plasma source, it is anticipated that the second spectrum of most of the metals will appear. Elements with higher ionization potentials may generate first spectra or perhaps a combination of both. A plasma source which produces a hotter plasma might enable the production of third and higher spectra. The lamp is admittedly a bit elaborate for a spectral lamp. Indeed, it was not designed for this purpose. It does offer certain advantages, however. Since the emission takes place in a free region, the hot metal plasma is never in contact with any component in the system. This should make this lamp useful for highly corrosive metals. Also, sputtering of electrode material into the discharge by heavy metallic ions is completely eliminated. In the present device, the rails are of Cu and no spectral lines of any species of Cu have appeared in any of the spectrograms. Depending on the gas used in the plasma gun and the rail material, very clean spectra probably can be obtained with little effort. The impurity lines in the present work arose apparently entirely from the machinable glass. These can probably be eliminated by replacing the Macor with a material more resistant to the plasma discharge. Quartz or, perhaps, a hard-fired ceramic might serve well for this purpose.

The plasma source used here performed reasonably well, but often displayed a temperamental and difficult-to-control nature.

This seems to be caused primarily by the irreproducibility of the pressure distribution between the rails immediately prior to ignition of the discharge. Better performance might be realized from a pulsed plasma source with a static gas pressure. A T-tube (Lincke and Griem 1966), for example, could be used. However, it is not known whether the Cs vapor source would operate in the relatively high pressure environment. Normally, T-tubes operate at static pressures on the order of a few Torr.

Alternatively, the plasma gun performance might be improved by a different valve. Gentry and Giese (1978) have created a fast pulsed gas valve which is quite similar to the one employed here. In this valve, however, the valve plate is an integral part of the discharge circuit. It is driven directly by the discharge current rather than being inductively coupled as in the valve used here. The direct coupling apparently makes the operation of the valve highly reliable and about 20 times more energy efficient than when inductive coupling is used. Another means of improving the performance of the plasma gun might be the use of a material other than Cu in the fabrication of the rails.

The method of analyzing the spectrograms to obtain relative intensities of lines is simple, reliable and generally applicable. Also, except for the method of estimating radial integrals, the theoretical development of the line strength expansion applies rigorously to a broad class of transitions. If it is modified to include transitions involving groups of equivalent electrons and to include

transitions of higher electromagnetic multipolarity, then the expressions are generally valid. These modifications are sufficiently complicated, however, that they warrant being done only to the extent necessary for specific cases. It is clear that the techniques and the apparatus described here could bear improvement, but it is equally clear that as they stand they are useful tools of atomic physics. This is supported by the analysis given in this dissertation of line strength ratios in Cs II.

APPENDIX A

NEW ENERGY LEVELS AND CLASSIFICATIONS IN CS II

Calculated energy levels of Cs II served as a guide in locating the five new levels reported in this appendix. The calculated energies used here are from the multiconfigurational Hartree-Fock analysis of Cs II by Reader (1976). The identification of these five remaining levels in the 5d configuration completes the energy level structure of Cs II for the configurations 5d, 6s, 6p, 6d and 7s. Three of the previously identified levels in the 6d configuration are due to Reader (1976). The rest are attributed to Wheatley and Sawyer (1942), but have been reinterpreted by Reader (1976).

The five new levels reported here were located by combining the wavelengths of previously unclassified transitions with known energy levels of the 6p and 7p configurations. Combinations of values were chosen which gave possible level energies in the vicinity of the predicted locations. In each case, several transitions were found to be in close agreement on the location of the level under consideration. The energy values obtained by this extensive numerical search accurately located the five new levels. The identification of each of the five levels is unambiguous. A situation in which two possible levels displayed equal merit never arose. The unclassified wavelengths used

in this search were drawn from Striganov and Sventitskii (1968, pp. 617-20), Harrison (1939), Balasse (1927) and Sommer (1924).

Table X displays the new energy levels in Cs II. The nominal $J_{1\ell}$ designations are based on the dominant composition amplitude as calculated by Reader (1976). Observed and calculated values are both given in cm^{-1} . The observed values are averages of the best agreement values found from the search. The values were weighted on the basis of the number of significant figures in the wavelength giving that value. The uncertainties shown in the table are RMS weighted deviations of the individual values from the weighted average. Once again, the weighting is based on the number of significant figures in the wavelength values.

The new energy levels permit the classification of 19 previously unclassified transitions in Cs II. Ten of these are 5d-6p and the remainder are 5d-7p. The new classifications are shown in Table XI. The designation assignments for the 6p and 7p levels are directly from Reader (1976). All wavelengths are air values in angstroms.

TABLE X. New Energy Levels in Cs II

Designation	Observed Level ^a	Calculated Level ^b
$5d \frac{1}{2} [1\frac{1}{2}]_2^0$	$128\,319.69 \pm 0.10$	128 291
$5d \frac{1}{2} [2\frac{1}{2}]_2^0$	$126\,697.17 \pm 0.55$	126 604
$5d \frac{1}{2} [2\frac{1}{2}]_3^0$	$129\,420.02 \pm 0.05$	129 390
$5d 1\frac{1}{2} [2\frac{1}{2}]_2^0$	$115\,675.37 \pm 0.33$	115 688
$5d 1\frac{1}{2} [2\frac{1}{2}]_3^0$	$118\,269.21 \pm 0.29$	118 281

^aUncertainties are RMS weighted deviations from weighted average level; see text for further discussion.

^bCalculated levels from Reader (1976).

TABLE XI. New Classifications in Cs II

Wavelength	Classification
6646.564	$5d \frac{1}{2} [1\frac{1}{2}]_2^0 - 6p \frac{1}{2} [1\frac{1}{2}]_1$
6627.77	- $6p \frac{1}{2} [1\frac{1}{2}]_2$
3614.989	- $7p 1\frac{1}{2} [1\frac{1}{2}]_1$
6724.476	$5d \frac{1}{2} [2\frac{1}{2}]_2^0 - 6p \frac{1}{2} [1\frac{1}{2}]_1$
5984.393	- $6p \frac{1}{2} [1\frac{1}{2}]_2$
3397.187	- $7p 1\frac{1}{2} [2\frac{1}{2}]_2$
3324.5	- $7p 1\frac{1}{2} [1\frac{1}{2}]_2$
7149.554	$5d \frac{1}{2} [2\frac{1}{2}]_3^0 - 6p \frac{1}{2} [1\frac{1}{2}]_2$
3655.73	- $7p 1\frac{1}{2} [1\frac{1}{2}]_2$
6979.681	$5d 1\frac{1}{2} [2\frac{1}{2}]_2^0 - 6p 1\frac{1}{2} [1\frac{1}{2}]_1$
3861.489	- $6p \frac{1}{2} [1\frac{1}{2}]_1$
3610.86	- $6p \frac{1}{2} [1\frac{1}{2}]_1$
3605.535	- $6p \frac{1}{2} [1\frac{1}{2}]_2$
2480.7	- $7p 1\frac{1}{2} [1\frac{1}{2}]_1$
2415.0	- $7p 1\frac{1}{2} [1\frac{1}{2}]_1$
3977.534	$5d 1\frac{1}{2} [2\frac{1}{2}]_3^0 - 6p \frac{1}{2} [1\frac{1}{2}]_2$
2641.0	- $7p 1\frac{1}{2} [2\frac{1}{2}]_2$
2613.6	- $7p 1\frac{1}{2} [2\frac{1}{2}]_3$
2596.95	- $7p 1\frac{1}{2} [1\frac{1}{2}]_2$

APPENDIX B

GENERAL SOLUTIONS OF THE RADIAL WAVE EQUATION

This appendix presents a brief evaluation of the general solutions of the radial wave equation,

$$\frac{d^2R(z)}{dz^2} + \left[-\frac{1}{4} + \frac{n}{z} - \frac{\ell(\ell + 1)}{z^2} \right] R(z) = 0. \quad (36)$$

Throughout the rest of this appendix, it is assumed that n and ℓ are any non-negative real numbers. If $n < 0$, then the transformation $z' = -z$ and the substitution $n' = -n$ puts the equation into the form considered here. If $\ell < 0$, then the substitution $\ell' = -\ell - 1$ may be used to obtain the appropriate expression.

The two independent solutions to equation (36) shall be specified by $R_1(z)$ and $R_2(z)$ with $R(z)$ being used where particular specification is unnecessary. The method of Frobenius may be used to find the general form of the solutions to equation (36). To implement this approach, the general solution is written as

$$R(z) = e^{-z/2} \left[z^\ell + 1 \left(\sum a_k z^k + \sum b_k z^k \right) + z^{-\ell} \sum c_k z^k \right], \quad (37)$$

where summation is over all values of the integer index k from zero to infinity.

Substitution of equation (37) into equation (36) yields the following relations among the coefficients:

$$\begin{aligned}
 a_0 &= 0, \quad 2\ell \neq 0, 1, 2, \dots \\
 a_0(2\ell + 1) + c_{2\ell}(n - \ell) &= 0, \quad 2\ell = 0, 1, 2, \dots,
 \end{aligned}
 \tag{38}$$

$$\begin{aligned}
 c_k &= 0, \quad k = 2\ell + 1 \\
 c_k(k - n - \ell) - c_{k+1}(k + 1)(k - 2\ell) &= 0, \quad k \neq 2\ell,
 \end{aligned}
 \tag{39}$$

$$a_k(k - n + \ell + 1) - a_{k+1}(k + 1)(k + 2\ell + 2) = 0, \tag{40}$$

and

$$\begin{aligned}
 b_k(k - n + \ell + 1) + a_k - a_{k+1}(2k + 2\ell + 3) \\
 - b_{k+1}(k + 1)(k + 2\ell + 2) &= 0.
 \end{aligned}
 \tag{41}$$

Actually, these relations, (38)-(41), with equation (37) give the most general form of the solutions to equation (36). It is worthwhile, however, to consider three particular cases that cover all the possible specific solutions that are conventionally used.

The first case occurs either when $n = \ell$ or when $2\ell \neq 0, 1, 2, \dots$ with arbitrary n . In this case, $a_k = 0$ for all k and the choices of c_0 and b_0 determine the forms of the independent solutions. For example, the choices $b_0 = 1$ and $c_0 = 0$, and $b_0 = 0$ and $c_0 = 1$ give, respectively,

$$R_1(z) = M_{n, \ell + \frac{1}{2}}(z), \tag{42}$$

$$R_2(z) = M_{n, -\ell - \frac{1}{2}}(z), \tag{43}$$

where the $M_{\mu, \nu}(z)$ are Whittaker functions (Whittaker and Watson 1927, pp. 337-38; Slater 1972, p. 505). Alternatively, the choices

$b_0 = \Gamma(-2\ell - 1)/\Gamma(-n - \ell)$ and $c_0 = \Gamma(2\ell + 1)/\Gamma(1 + \ell - n)$, and $b_0 = \Gamma(2\ell + 1)/\Gamma(1 + \ell - n)$ and $c_0 = \Gamma(-2\ell - 1)/\Gamma(-n - \ell)$ give, respectively,

$$R_1(z) = W_{n, \ell + \frac{1}{2}}(z), \quad (44)$$

and

$$R_2(z) = W_{-n, \ell + \frac{1}{2}}(-z), \quad (45)$$

where the $W_{\mu, \nu}(z)$ are also Whittaker functions (Whittaker and Watson 1927, pp. 339-40 and 343; Slater 1972, p. 505).

The second case is realized when $2\ell = 0, 1, 2, \dots$ and $n - \ell - 1 \neq 0, 1, 2, \dots$. This case pertains directly to the Coulomb approximation (Bates and Damgaard 1949), in general. The conventional solutions are found here by specifying a_0 and b_0 . For $a_0 = 0$ and $b_0 = 1$, the first solution appears as

$$R_1(z) = M_{n, \ell + \frac{1}{2}}(z). \quad (46).$$

This solution is regular at the origin and diverges as z tends to infinity. The second solution which is regular at infinity and divergent at the origin is the function used by Bates and Damgaard (1949) to approximate radial wave functions. It follows from the selections $a_0 = 1/[2\ell + 1]!\Gamma(-n - \ell)$ and $b_0 = a_0[\psi(\ell + 1 - n) - \psi(1) - \psi(2\ell + 2)]$ where $\psi(z)$ is the digamma function (Davis 1972, p. 258). The second solution for this case is

$$\begin{aligned}
R_2(z) &= W_{n, \ell + \frac{1}{2}}(z) \\
&= \frac{e^{-z/2} z^{\ell+1}}{(2\ell+1)! \Gamma(-n-\ell)} \{ \ell n z {}_1F_1(\ell+1-n; 2\ell+2; z) \\
&+ \sum_{k=0}^{\infty} \frac{(\ell+1-n)_k}{k!(2\ell+2)_k} z^k [\psi(k-n+\ell+1) - \psi(k+1) \\
&- \psi(k+2\ell+2)] \} + \frac{e^{-z/2} z^{-\ell}}{\Gamma(\ell+1-n)} \sum_{k=0}^{2\ell} \frac{(-n-\ell)_k (2\ell-k)!}{k!} (-z)^k,
\end{aligned} \tag{47}$$

where ${}_1F_1(a;b;z)$ is the confluent hypergeometric function (Landau and Lifshitz 1975, pp. 600-04), and where $(z)_k$ is the Pochhammer symbol (Davis 1972, p. 256). Rather than use the formidable expression in equation (47), Bates and Damgaard (1949) opt for the much simpler asymptotic expansion of this function for large z . The unnormalized form here is

$$W_{n, \ell + \frac{1}{2}}(z) \sim e^{-z/2} z^n \sum_{k=0}^{\infty} \frac{(\ell+1-n)_k (-n-\ell)_k}{k!} \left(\frac{-1}{z}\right)^k. \tag{48}$$

The third, and final, case corresponds to $2\ell = 0, 1, 2, \dots$ and $n - \ell - 1 = 0, 1, 2, \dots$. The familiar eigenvalue problem is a member of this case. The solutions derived below are applicable to exact hydrogenic calculations and to the ECP approximation. Conventionally, the first solution follows from $a_0 = 0$ and $b_0 = 1$ which yield

$$\begin{aligned}
R_1(z) &= M_{n, \ell + \frac{1}{2}}(z) \\
&= e^{-z/2} z^{\ell+1} {}_1F_1(\ell+1-n; 2\ell+2; z).
\end{aligned} \tag{49}$$

This is probably the most familiar solution in this appendix. It is the unnormalized form of the hydrogenic radial wave function (Landau

and Lifshitz 1975, p. 119; Condon and Shortley 1970, p. 115). The solution shown in equation (49) is the only solution for $2\ell = 0, 1, 2, \dots$ which is regular at both zero and infinity. This accounts for its utility in representing physical systems. It also shows the necessity of integer values of n , such that $n - \ell - 1 = 0, 1, 2, \dots$, for physical systems described exactly by equations of the form of equation (36). Noninteger values of n lead to representations of physical systems which are of necessity approximate and which must be truncated at either large or small values of z depending on the chosen solution. It is interesting to note, however, that if 2ℓ and n are both noninteger and if ℓ and n have fractional parts of equal magnitude, then solutions that are regular at zero and infinity arise from equation (42) of the first case considered here. Thus, equation (49) might not be the only solution given here which is capable of representing a real physical system exactly.

Strangely enough, the second solution corresponding to the popular equation (49) is certainly the least familiar of all the solutions considered here. Since equation (49) is regular at both zero and infinity, the second solution here must be divergent at both zero and infinity. This undesirable behavior has made this second solution singularly unpopular. This appendix may well be its first public appearance. In this case, the second solution follows from the choices $a_0 = 1/[(2\ell + 1)!(n - \ell - 1)!]$ and $b_0 = a_0[\psi(n - \ell) - \psi(1) - \psi(2\ell + 2)]$. It is

$$\begin{aligned}
R_2(z) = & \frac{e^{-z/2} z^{\ell+1}}{(2\ell+1)!(n-\ell-1)!} \{ \ln z {}_1F_1(\ell+1-n; 2\ell+2; z) \\
& + \sum_{k=0}^{n-\ell-1} \frac{(\ell+1-n)_k}{k!(2\ell+2)_k} z^k [\psi(n-\ell-k) - \psi(k+1) \\
& - \psi(k+2\ell+2)] \} - e^{-z/2} z^{-\ell} \sum_{k=0}^{2\ell} \frac{(2\ell-k)!}{k!(n+\ell-k)!} z^k \\
& + \frac{(-)^{n-\ell-1} e^{-z/2} z^{n+1}}{(n+\ell+1)!(n-\ell)!} {}_2F_2(1,1; n-\ell+1, n+\ell+2; z), \quad (50)
\end{aligned}$$

where ${}_2F_2(a,b;c,d;z)$ is a generalized hypergeometric function (Lebedev 1972). This concludes the presentation of the general solutions to the radial wave equation (36). As has been shown above, all the myriad conventional solutions follow from equation (37) and the relations (38)-(41) as various special cases of this general solution.

REFERENCES

- Anderson, David K., Douglas W. Jones and J. D. McCullen, *Rev. Sci. Instrum.* 48, 1361 (1977).
- Balasse, M. G., *J. Phys. Radium* 8, 311 (1927).
- Bates, D. R. and Agnete Damgaard, *Philos. Trans. R. Soc. Lond. A* 242, 101 (1949).
- Brink, D. M. and G. R. Satchler, Angular Momentum (Clarendon, Oxford, 1968).
- Burgess, A. and M. J. Seaton, *Mon. Not. R. Astron. Soc.* 120, 121 (1960).
- Condon, E. U. and G. H. Shortley, The Theory of Atomic Spectra (Cambridge Univ., London, 1970).
- Davis, Philip J., in Handbook of Mathematical Functions, edited by Milton Abramowitz and Irene A. Stegun (Dover, New York, 1972), Chap. 6.
- Gentry, W. Ronald and Clayton F. Giese, *Rev. Sci. Instrum.* 49, 595 (1978).
- Gordon, W. *Ann. Phys. (Leipz.)* 2, 1031 (1929).
- Griem, Hans R., Plasma Spectroscopy (McGraw-Hill, New York, 1964).
- Harrison, George R., MIT Wavelength Tables (MIT Press, Cambridge, Mass., 1939).
- Hartree, D. R., *Proc. Camb. Philos. Soc.* 24, 89 (1927).
- Kodak Plates and Films for Scientific Photography, 1st ed., Publication No. P-315 (Eastman Kodak, Rochester, N.Y., 1973).
- Landau, L. D. and E. M. Lifshitz, Quantum Mechanics, 2nd ed. (Pergamon, Oxford, 1975).
- Lebedev, N. N., Special Functions and Their Applications (Dover, New York, 1972) p. 275.
- Lincke, R. and H. R. Griem, *Phys. Rev.* 143, 66 (1966).

- Olthoff, J. and R. A. Sawyer, *Phys. Rev.* 42, 766 (1932).
- Ramsey, Norman F., Molecular Beams (Oxford Univ., London, 1956), p. 379.
- Reader, Joseph, *Phys. Rev. A* 13, 507 (1976).
- Reader, Joseph, private communication (1978).
- Reader, Joseph and Gabriel L. Epstein, *J. Opt. Soc. Am.* 65, 638 (1975).
- Slater, Lucy Joan, in Handbook of Mathematical Functions, edited by Milton Abramowitz and Irene A. Stegun (Dover, New York, 1972), Chap. 13.
- Sobel'man, I. I., Introduction to the Theory of Atomic Spectra (Pergamon, Oxford, 1972).
- Sommer, L. A., *Ann. Phys. (Leipz.)* 75, 163 (1924).
- Striganov, A. R. and N. S. Sventitskii, Tables of Spectral Lines of Neutral and Ionized Atoms (IFI/Plenum, New York, 1968).
- Wheatley, Marshall A. and Ralph A. Sawyer, *Phys. Rev.* 61, 591 (1942).
- Whittaker, E. T. and G. N. Watson, A Course of Modern Analysis, 4th ed. (Cambridge Univ., London, 1927).